Performance Analysis for RIS-Assisted SWIPT-Enabled IoT Systems

Bingxin Zhang, *Student Member, IEEE,* Kun Yang, *Fellow, IEEE,* Kezhi Wang, *Senior Member, IEEE,* and Guopeng Zhang

***Abstract*—Reconfigurable intelligent surface (RIS) is a promising technology to improve the spectral and energy efficiency of Internet of Things (IoT) systems. In this paper, we investigate an RIS-assisted simultaneous wireless information and power transmission (SWIPT) system by utilizing stochastic geometry. Moreover, we consider not only the case of random phase shift, but also the case where the phase shift of the RIS are aligned to the k-th IoT device. We first derive the closed-form expressions of the uplink outage probability and the average uplink data size for the k-th IoT device under the Rayleigh channel. Then, we extend the performance analysis to the Rician fading channel and multi-antenna scenarios. Finally, extensive numerical results have been carried out to verify the effectiveness of our derived results.**

***Index Terms*—Reconfigurable intelligent surface, simultaneous wireless information and power transfer, outage probability, stochastic geometry.**

I. Introduction

In the future communication networks, comprehensive monitoring and sensing of the real world will be achieved through various sensors [1]. The deployment and maintenance of a large number of wireless sensors will be required across diverse scenarios. Nevertheless, how to provide continuous and stable energy for these wireless sensors to maintain reliable information transmission has become an urgent issue to be resolved. Therefore, the research on simultaneous wireless information and power transfer (SWIPT) has attracted widespread attention, especially for energy constrained systems and various Internet of Things (IoT) applications. Specifically, in the SWIPT system, using a practical scheme such as time-switching or power-splitting (PS), information decoding (ID) and energy harvesting (EH) can be performed simultaneously at receivers exploiting the power of the electromagnetic waves [2]. Wireless receivers can utilize the energy harvested from radio frequency (RF) signals to enhance their stability and reliability of operation [3]. In [4], the authors investigated the fundamental limits of SWIPT systems over a Rayleigh fading channel, and found that high-power amplifier significantly reduces the information-energy capacity region. The authors in [5] provided a SWIPT scheme for the IoT. To reduce the interference and improve the power amplifier efficiency, this scheme sends information via utilizing a small modulated signal and transmits the wireless power by the unmodulated high-power continuous wave. The authors in [6] considered a receive spatial modulation assisted SWIPT system with finite alphabets, and theoretically analyzed the performance of three different transmission schemes. In [7], the authors analyzed the performance of SWIPT in systems employing cooperative non-orthogonal multiple access (NOMA) with imperfect channel state information (CSI). The authors in [8] studied the rate-energy trade-off and decoding error probability-energy trade-off for SWIPT in finite codelength. This is different from any work that assumes infinite codelength. Nevertheless, in some complex scenarios, such as automated factory, wireless signals are more likely to be blocked due to the densely deployed equipment and thick walls/pillars, which leads to IoT devices being unable to enjoy the benefits of SWIPT.

Recently, deploying reconfigurable intelligent surfaces (RISs) in the existing wireless system is a promising solution to address this problem. More specifically, the RIS is a low-cost meta-surface consisting of a massive number of elements, which can intelligently adjust the phase and/or amplitude response with the help of a programmable controller to modify the reflection behavior of the incident wave to improve the spectral efficiency and coverage of wireless communication systems [9], [10].

Inspired by its numerous potential advantages, RIS-assisted wireless systems have been studied in different communication scenarios [11]–[19]. The authors in [11] proposed a strategy in which the elements of the RIS only require to introduce random phase rotation in each coherence interval without any CSI. For the finite blocklength regime, the authors in [12] evaluated the performance of an RIS-assisted ultra-reliable and low-latency communication by studying the average achievable rate and error probability, while the authors in [13] further investigated wireless energy transfer technology in the system. In [14], a framework for RIS-aided unmanned aerial vehicle enabled networks was studied. Within this framework, the authors solved an optimization problem aimed to minimizing energy consumption by jointly designing multiple variables. For mobility scenarios, the authors in [15] investigated a

This paper was partly funded by MOST Major Research and Development Project (Grant No.: 2021YFB2900204), Natural Science Foundation of China (No. 62132004, 61971102), UESTC Yangtze Delta Region Research Institute-Quzhou (No. 2022D031, 2023D005). (*Corresponding author: Kun Yang*)

Bingxin Zhang is with the School of Information and Communication Engineering, University of Electronic Science and Technology of China, Chengdu 611731, China (e-mail: bxzhang@std.uestc.edu.cn).

Kun Yang is with the School of Information and Communication Engineering and Yangtze Delta Region Research Institute, University of Electronic Science and Technology of China, Chengdu 611731, China, and also with the School of Intelligent Software and Engineering, Nanjing University, Suzhou 215163, China (e-mail: kyang@ieee.org).

Kezhi Wang is with Department of Computer Science, Brunel University London, Uxbridge, Middlesex, UB8 3PH (email: kezhi.wang@brunel.ac.uk).

Guopeng Zhang is with the School of Computer Science and Technology, China University of Mining and Technology, Xuzhou 221116, China (e-mail: gpzhang@cumt.edu.cn).

novel RIS-aided high-mobility wireless communication system, which combines many refracting elements with a high-speed vehicle to assisted the communication between a remote base station (BS) and users. In [16], the authors studied an RIS-assisted hybrid automatic repeat request system with incremental redundancy. Specifically, the authors derived expressions for the outage probability of the network under single-input single-output and single-input multiple-output (SIMO) scenarios by considering the Rician channel and multiple RISs. In [17], the authors developed a hybrid multi-objective evolutionary paradigm to reduce the training overhead of millimeter wave channels in IRS-aided multi-input multi-output (MIMO) systems. In [18], the authors analyzed the performance of an RIS-assisted NOMA system in both the best-case and worst-case by deriving the outage probability and the ergodic rate of the user. The authors in [19] introduced a universal framework aimed to improving the transmit power efficiency in RIS-assisted multi-group NOMA networks. This enhancement is achieved within the context of coordinated multi-point reception, while considering the challenges posed by imperfect successive interference cancellation. In addition, some work studied the random distribution of IoT devices' locations in the RIS-aided network [20]–[24]. In particular, in our previous work [24], we analyzed the RIS-assisted wireless communication system with energy harvesting. However, the paper only studied the performance of energy harvesting in IoT devices, without considering how to actively utilize the harvested energy.

There has been many works on the RIS-assisted SWIPT system [25]–[31]. The authors in [25] studied a multi-user intelligent reflecting surface assisted SWIPT system. This work aimed to maximize the weighted sum rate of the information receiver by jointly optimizing the transmission precoding matrix of the BS and the passive phase shifting matrix of the RIS. In [26], the authors aimed to minimize the transmit power at an multi-antenna access point by jointly designing active and passive beamforming while meeting the users' quality-of-service. Furthermore, the authors in [27] and [28] explored the joint hybrid beamforming with discrete phase shift design in an RIS-aided SWIPT system. In [29], the authors proposed an optimal resource allocation algorithm for large intelligent reflecting surface aided SWIPT systems, and developed a scalable optimization framework to facilitate efficient system design. The authors in [30] improved the performance of NOMA and the wireless power transfer efficiency of SWIPT by deploying an intelligent reflecting surfaces. The authors in [31] considered an intelligent reflecting surfaces-assisted wireless powered mobile edge computing system and proposed a computing offloading framework. Specifically, the authors conducted a comprehensive analysis and comparison of the computational offloading schemes under time-division multiple access (TDMA) and NOMA. However, the current work mainly focused on the optimization of the system and ignores the in-depth performance analysis of the RIS-assisted SWIPT system. Especially, none of the above work considered that IoT devices are usually randomly distributed in practical applications.

Motivated the above, we propose an RIS-assisted SWIPT IoT system, where the location of IoT devices is modeled as a homogeneous Poisson point process (PPP). In this system, the BS usually needs to send control information or commands in the form of multicast to IoT devices scattered on the ground [32]. For instance, they may multicast control commands to all IoT devices, instructing them to upload the information they have collected. Then, the IoT devices transmit the environmental information collected over a period of time to the BS. Meanwhile, the vast majority of IoT devices are powered by batteries. Once the batteries are depleted, they will be unable to operate normally. However, they can harvest the power of the downlink radio frequency signals sent by the BS in multicast form. Therefore, we divide the whole period into two transmission phases, as shown in Fig. 1(b). In the downlink transmission phase, part of the received power is used for ID, while the other part is utilized for EH. In the uplink transmission phase, we use the TDMA protocol to improve system compatibility, bandwidth efficiency, reliability, and cost-effectiveness. This is especially beneficial in low-power IoT systems operating in challenging environments. Specifically, the main contributions are summarized as follows:

- We first derive the closed-form expressions of the uplink outage probability for the k-th IoT device with random and optimal phase shift models under the Rayleigh channel condition. Moreover, by taking the Poisson distributed number of IoT devices into consideration, we derived the exact expression of the average uplink data size for the k-th IoT device under the case of random phase shift. In particular, when the phase shift of RIS are just aligned to the k-th IoT device, an upper bound of average uplink data size is derived by exploiting the Jensen's inequality.
- We further extend the performance analysis of the system to the Rician fading channel and multi-antenna scenarios. Specifically, we characterize the statistical features of the channel gain in these two scenarios. Based on the obtained results, we derive the closed-form expressions for the uplink outage probability and the average uplink data size of the k-th IoT device in these two scenarios.
- Finally, extensive simulations are provided to demonstrate the accuracy of the derived results. In addition, we provide several insights by analyzing the impact of parameters on the system performance. Specifically, increasing the transmit power and the number of antennas of the BS or the number of reflection elements can significantly improve the system performance. However, with the increase of density of IoT devices, the system performance deteriorates gradually.

The rest of this paper is organized as follows. In Section II, the system model with RIS-assisted SWIPT system is introduced. Section III and IV are devoted to performance analysis for the downlink and uplink transmission, respectively. The numerical results are presented in Section V to validate the correctness of theoretical analysis results. Finally, the conclusion is drawn in Section VI.

II. System model

In this work, we study an RIS-aided SWIPT system, as shown in Fig. 1(a), which consists a BS, a group of IoT

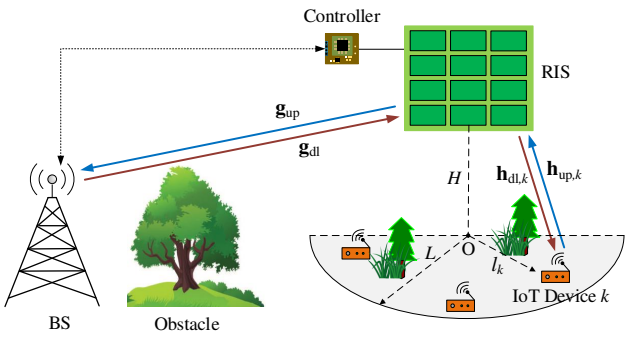

(a)

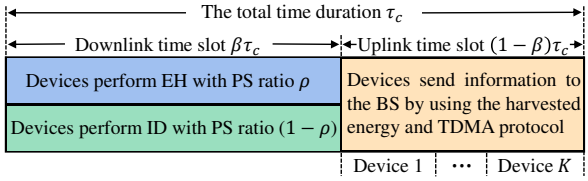

(b)

Fig. 1: The RIS-assisted SWIPT in the low-power IoT system.

devices and an RIS with N reflecting elements. In some special scenarios, such as mountain areas, battlefields, or forest plantations, IoT devices may be far away from the BS. Specifically, the direct links between IoT devices on the ground and the BS may be blocked by trees. Therefore, we assume that the links between the BS and IoT devices can only be established through the RIS. We also assume that the RIS is located in close proximity of the IoT devices and exclusively serves the IoT devices within a limited geographical area [33].

In general, due to the inherent properties of the RIS, it can only reflect signals for IoT devices located in its front half-space. Therefore, as depicted in Fig. 1(a), we assume that IoT devices are deployed in a semicircular area centered on the projection point of the RIS on the ground plane. The radius of this semicircular area is denoted by L. The location of IoT devices is modeled as a homogeneous PPP with density λ. The number of IoT devices, denoted by K ($K \geq 1$), is Poisson distributed i.e., $P\{K = q\} = \frac{\mu^q e^{-\mu}}{q!}$, where $\mu = \frac{\pi L^2 \lambda}{2}$ is the mean measure. As the k-th IoT device follows uniform distribution in the area covered by the RIS, the cumulative distribution function (CDF) of l_k can be derived as

$$F_{l_k}(x) = \int_0^{\pi} \int_0^{x} \frac{l}{\frac{1}{2}\pi L^2} \mathrm{d}l\mathrm{d}\theta = \frac{x^2}{L^2}, \forall x \in [0, L], \quad (1)$$

where l_k is the distance from the k-th IoT device to the projection point of the RIS on the ground plane. Let H represent the vertical height of the RIS, d_{SR} represent the distance from the BS to the RIS, and d_k is the distance from the RIS to the k-th IoT device. As a result, one has $d_k = \sqrt{H^2 + l_k^2}$. Then, the CDF of d_k can be derived as

$$\begin{aligned} F_{d_k}(x) &= \Pr\{\sqrt{H^2 + l_k^2} < x\} = \Pr\left\{l_k < \sqrt{x^2 - H^2}\right\} \\ &= F_{l_k}(\sqrt{x^2 - H^2}) = \frac{x^2 - H^2}{L^2}, \end{aligned} \quad (2)$$

where $H = d_{\min} \leq x \leq d_{\max} = \sqrt{H^2 + L^2}$.

Taking the first-order derivative of (2), the probability density function (PDF) of d_k can be given by

$$f_{d_k}(x) = \frac{2x}{L^2}. \quad (3)$$

Furthermore, an illustration of the transmission protocol is depicted in Fig. 1(b). It is assumed that the total transmission duration for downlink and uplink is τ_c. Let $\beta\tau_c$ and $(1-\beta)\tau_c$ denote the downlink transmission time for the BS and the uplink transmission time for each IoT device, respectively, where $\beta \in (0, 1)$ is the time allocation factor. For practical applications, we consider that each IoT device is equipped with a battery, which can storage the energy harvested. We employ the "harvest-then-transmit" protocol in the RIS-assisted system, which means that IoT devices can harvest energy during the downlink transmission period and then send their data to the BS with the help of RIS during the uplink transmission period. In the uplink transmission phase, the TDMA protocol is employed. Therefore, each IoT device transmits its own data to the BS within the time interval of $[(1-\beta)\tau_c/K]$. We assume that the receiver of each IoT device has a power-splitting architecture with a PS ratio $\rho \in (0, 1)$. In other words, the ρ portion of the received power is utilized for EH, while $(1-\rho)$ portion of the power is utilized for ID.

Assuming that all wireless links are experience independent Rayleigh fading [22]. The complex channel coefficient vectors from the BS to the RIS, from the RIS to the k-th IoT device, from the k-th IoT device to the RIS and from the RIS to the BS are represented by $\mathbf{g}_{\text{dl}} = [g_{\text{dl},1}, ..., g_{\text{dl},N}]^{\text{H}}$, $\mathbf{h}_{\text{dl},k} = [h_{\text{dl},k,1}, ..., h_{\text{dl},k,N}]^{\text{H}}$, $\mathbf{h}_{\text{up},k} = [h_{\text{up},k,1}, ..., h_{\text{up},k,N}]^{\text{H}}$ and $\mathbf{g}_{\text{up}} = [g_{\text{up},1}, ..., g_{\text{up},N}]^{\text{H}}$, respectively, where $g_{\text{dl},n}$, $h_{\text{dl},k,n}$, $h_{\text{up},k,n}$ and $g_{\text{up},n} \sim \mathcal{CN}(0, 1)$. $\mathbf{\Phi}_{\text{up}} = \text{diag}(\varrho_{\text{up},1} e^{j\phi_{\text{up},1}}, ..., \varrho_{\text{up},N} e^{j\phi_{\text{up},N}})$ and $\mathbf{\Phi}_{\text{dl}} = \text{diag}(\varrho_{\text{dl},1} e^{j\phi_{\text{dl},1}}, ..., \varrho_{\text{dl},N} e^{j\phi_{\text{dl},N}})$ denote the diagonal reflection coefficient matrices for uplink and downlink transmission phase, respectively, where $\phi_{\text{up},n} \in [0, 2\pi)$ and $\phi_{\text{dl},n} \in [0, 2\pi)$ are the phase shift of the n-th reflecting element of the RIS, and $\varrho_{\text{up},n} \in [0, 1]$ and $\varrho_{\text{dl},n} \in [0, 1]$ are the corresponding amplitude. In Particular, we assume $\varrho_{\text{dl},n} = \varrho_{\text{up},n} = 1$ to obtain the traceable results and maximize the signal reflection [22]. Additionally, we consider the performance analysis of RIS-assisted low-power IoT systems under two different phase shift, namely the random phase shift model and the optimal phase shift model. For random phase shift model, the phase shift of elements is randomly selected. This is because in some complex scenarios, it is difficult to obtain available CSI, so that the phase shift matrix is assumed to be randomly designed. For the optimal phase shift model, we assume that the phase shifts of all elements are just aligned with the k-th IoT device, i.e., $\phi_{\text{up},n} = -\arg(h_{\text{up},k,n}) - \arg(g_{\text{up},n})$ and $\phi_{\text{dl},n} = -\arg(h_{\text{dl},k,n}) - \arg(g_{\text{dl},n})$.

In the downlink transmission phase, the BS multicasts the same information to all IoT devices. There is no inter-user interference in multicast communication systems due to multiple IoT devices sharing the same information. Therefore, the received signal at the k-th IoT device in the downlink

transmission phase can be written as

$$y_{\mathrm{dl},k} = \sqrt{P_{\mathrm{T}} d_{\mathrm{SR}}^{-\alpha} d_k^{-\alpha}} \mathbf{g}_{\mathrm{dl}}^{\mathrm{H}} \mathbf{\Phi}_{\mathrm{dl}} \mathbf{h}_{\mathrm{dl},k} x_{\mathrm{dl}} + w_{\mathrm{dl},k}, \tag{4}$$

where P_{T} is the transmit power of the BS, α denotes the path-loss exponent, x_{dl} is the information symbol with and $w_{\mathrm{dl},k} \sim \mathcal{CN}(0, \sigma_{\mathrm{dl},k}^2)$ is the additive white Gaussian noise (AWGN) at the k-th IoT device.

According to the transmission protocol depicted in Fig. 1(b), each IoT device adopts the PS scheme to coordinate the process of ID and EH for the received signal in the downlink transmission period. The $(1-\rho)$ portion of the received power is utilized for ID. Therefore, the instantaneous signal-to-noise ratio (SNR) at the k-th IoT device is given by

$$\gamma_{\mathrm{dl},k} = \frac{(1-\rho) P_{\mathrm{T}} \left| \mathbf{g}_{\mathrm{dl}}^{\mathrm{H}} \mathbf{\Phi}_{\mathrm{dl}} \mathbf{h}_{\mathrm{dl},k} \right|^2}{\sigma_{\mathrm{dl},k}^2 d_{\mathrm{SR}}^{\alpha} d_k^{\alpha}} = \varphi_0 d_k^{-\alpha} \Lambda_{\mathrm{dl},k}, \tag{5}$$

where $\varphi_0 = \frac{(1-\rho)P_{\mathrm{T}}}{d_{\mathrm{SR}}^{\alpha} \sigma_{\mathrm{dl},k}^2}$ and $\Lambda_{\mathrm{dl},k} = \left| \mathbf{g}_{\mathrm{dl}}^{\mathrm{H}} \mathbf{\Phi}_{\mathrm{dl}} \mathbf{h}_{\mathrm{dl},k} \right|^2$.

For the k-th IoT device, the ρ portion of the received power is used for EH. Moreover, it can be considered that the energy obtained from the noise is negligible. Accordingly, the instantaneous harvested power of the k-th IoT device in the downlink transmission can be given by

$$P_{\mathrm{EH},k} = \eta \rho P_{\mathrm{T}} d_{\mathrm{SR}}^{-\alpha} d_k^{-\alpha} \Lambda_{\mathrm{dl},k}, \tag{6}$$

where $0 < \eta < 1$ is the energy conversion efficiency of IoT devices.

In contrast to the traditional communication systems, the cost of ID can not be ignored in low-power SWIPT IoT systems. According to [34], the total power consumption of the k-th IoT device can be modeled as $P_{\mathrm{C},k} = P_{\mathrm{D},k} + P_{\mathrm{F},k}$, where $P_{\mathrm{D},k}$ denotes the power consumption required for ID and $P_{\mathrm{F},k}$ is the fixed circuit power consumption to maintain the operation of the k-th IoT device. Specifically, the exponential decoding power consumption of the k-the IoT device can be given by

$$P_{\mathrm{D},k} = \varpi \left(2^{R_{\mathrm{dl},k}} - 1 \right) = \varpi \gamma_{\mathrm{dl},k}, \tag{7}$$

where $R_{\mathrm{dl},k} = \log_2 \left(1 + \gamma_{\mathrm{dl},k} \right)$ is the downlink ID rate of the k-th IoT device and ϖ is a constant coefficient [34]. In particular, the circuit power consumption is ignored in the paper due to its relatively small constant relative to the decoding power consumption.

Therefore, according to the TDMA protocol in the uplink transmission phase, the average transmit power of the k-th IoT device can be expressed as

$$\begin{aligned} P_{\mathrm{A},k} &= \frac{\beta \tau_c K}{(1-\beta)\tau_c} \left(P_{\mathrm{EH},k} - P_{\mathrm{D},k} \right) \\ &= \frac{\beta K}{(1-\beta)} \left(\frac{\eta \rho P_{\mathrm{T}} \Lambda_{\mathrm{dl},k}}{d_{\mathrm{SR}}^{\alpha} d_k^{\alpha}} - \frac{\varpi (1-\rho) P_{\mathrm{T}} \Lambda_{\mathrm{dl},k}}{\sigma_{\mathrm{dl},k}^2 d_{\mathrm{SR}}^{\alpha} d_k^{\alpha}} \right). \end{aligned} \tag{8}$$

Hence, the signal of the k-th IoT device received by the BS in the uplink transmission phase can be expressed as

$$y_{\mathrm{up},k} = \sqrt{P_{\mathrm{A},k} d_{\mathrm{SR}}^{-\alpha} d_k^{-\alpha}} \mathbf{g}_{\mathrm{up}}^{\mathrm{H}} \mathbf{\Phi}_{\mathrm{up}} \mathbf{h}_{\mathrm{up},k} x_{\mathrm{up},k} + w_{\mathrm{up},k}, \tag{9}$$

where $x_{\mathrm{up},k}$ is the information symbol of the k-th IoT device with $\mathbb{E}\{||x_{\mathrm{up},k}||^2\} = 1$ and $w_{\mathrm{up},k} \sim \mathcal{CN}(0, \sigma_{\mathrm{up}}^2)$ is the AWGN.

Then, based on (8), the SNR of the k-th IoT device in the uplink transmission phase can be written as

$$\begin{aligned} \gamma_{\mathrm{up},k} &= \frac{P_{\mathrm{A},k} \left| \mathbf{g}_{\mathrm{up}}^{\mathrm{H}} \mathbf{\Phi}_{\mathrm{up}} \mathbf{h}_{\mathrm{up},k} \right|^2}{d_{\mathrm{SR}}^{\alpha} d_k^{\alpha} \sigma_{\mathrm{up}}^2} \\ &= \frac{\beta K P_{\mathrm{T}}}{(1-\beta) d_{\mathrm{SR}}^{2\alpha} \sigma_{\mathrm{up}}^2} \left(\eta \rho - \frac{\varpi (1-\rho)}{\sigma_{\mathrm{dl},k}^2} \right) \frac{\Lambda_{\mathrm{dl},k} \Lambda_{\mathrm{up},k}}{d_k^{2\alpha}}, \end{aligned} \tag{10}$$

where $\Lambda_{\mathrm{up},k} = \left| \mathbf{g}_{\mathrm{up}}^{\mathrm{H}} \mathbf{\Phi}_{\mathrm{up}} \mathbf{h}_{\mathrm{up},k} \right|^2$.

III. Performance analysis of uplink transmission

As shown in Fig. 1(b), by applying the PS scheme, one part of the signal power in the downlink transmission phase is allocated to decode information, while the other part is allocated to EH. The ID performance of the downlink has been extensively analyzed in numerous literature, and thus, this paper does not focus on its analysis. Instead, we focus on the performance of IoT devices in sending data to the BS using the harvested energy during the uplink transmission phase. Specifically, considering the Poisson distribution of the number of IoT devices, we analyze the system performance in terms of uplink outage probability and average uplink data size for the k-th IoT device.

In this paper, we study two phase shift models, namely the random phase shift model and the optimal phase shift model. We take the performance of these two models as the theoretical lower and upper bounds for the k-th IoT device, respectively. Specifically, in the random phase shift model, we consider that the phase shifts randomly generated by the RIS are not aligned with the k-th IoT device during both uplink and downlink transmission phases, resulting in the worst performance. Under the optimal phase shift model, we assume that the phase shifts of the RIS are just aligned with the k-th IoT device, resulting in the best performance. For further analysis, we first determine the statistical features of channel gain under these two phase shift models.

Based on [35], for the random phase shift, the PDF and CDF of the downlink channel gain $\Lambda_{\mathrm{dl},k}^{\mathrm{R}}$ are respectively given by

$$\begin{aligned} f_{\Lambda_{\mathrm{dl},k}^{\mathrm{R}}} &= \frac{2 x^{\frac{N-1}{2}}}{\Gamma(N)} K_{N-1} \left(2\sqrt{x} \right), \\ F_{\Lambda_{\mathrm{dl},k}^{\mathrm{R}}} &= 1 - \frac{2}{\Gamma(N)} x^{\frac{N}{2}} K_N \left(2\sqrt{x} \right), \end{aligned} \tag{11}$$

where $\Gamma(\cdot)$ denotes the gamma function and $K_{\vartheta}(\cdot)$ is the ϑ-th order modified Bessel function of the second kind.

According to [36], for the optimal phase shift model, the statistical characteristics of the downlink channel gain $\Lambda_{\mathrm{dl},k}^{\mathrm{O}}$ can be respectively given by

$$\begin{aligned} f_{\Lambda_{\mathrm{dl},k}^{\mathrm{O}}}(x) &= \frac{1}{\Gamma(\zeta) \theta^{\zeta}} x^{\zeta - 1} e^{-\frac{x}{\theta}}, \\ F_{\Lambda_{\mathrm{dl},k}^{\mathrm{O}}}(x) &= \frac{1}{\Gamma(\zeta)} \Upsilon \left(\zeta, \frac{x}{\theta} \right), \end{aligned} \tag{12}$$

where $\zeta = \frac{u_X^2}{v_X - u_X^2}$, $\theta = \frac{v_X - u_X^2}{u_X}$ and $\Upsilon(\cdot,\cdot)$ represents the lower incomplete Gamma function. Specifically, u_X and v_X follow from [36, Eq. (A5)].

Note that based on channel reciprocity, the channel gain $\Lambda_{\mathrm{up},k}$ in the uplink transmission phase has the same statistical characteristics as $\Lambda_{\mathrm{dl},k}$ in the downlink transmission phase.

A. The uplink outage probability of the k-th IoT device

Based on (10), the uplink outage probability of the k-th IoT device is defined as

$$\begin{aligned} P_{\mathrm{up},k} &= \Pr\left\{\log_2\left(1+\gamma_{\mathrm{up},k}\right) < C_{\mathrm{up,th}}\right\} \\ &= \Pr\left\{\frac{\eta\rho P_t K\beta\Lambda_{\mathrm{dl},k}\Lambda_{\mathrm{up},k}}{(1-\beta)\sigma_{\mathrm{up}}^2 d_{\mathrm{SR}}^{2\alpha} d_k^{2\alpha}} < \Theta_{\mathrm{up}}\right\}, \end{aligned} \tag{13}$$

where $\Theta_{\mathrm{up}} = 2^{C_{\mathrm{up,th}}} - 1$ and $C_{\mathrm{up,th}}$ denotes an uplink rate threshold. It should be noted that $C_{\mathrm{up,th}}$ is a value in direct proportion to the number of IoT devices. This is because more IoT devices shorten the time for each IoT device to transmit data information. Therefore, a higher data rate is required to ensure successful transmission.

Lemma 1. Based on (11) and (13), the closed-form expression of uplink outage probability for the k-th IoT device in the case of random phase shift can be written as

$$\begin{aligned} P_{\mathrm{up},k}^{\mathrm{R}} = \sum_{K=1}^{\Xi}\frac{\mu^K e^{-\mu}}{K!}\Bigg\{1 - \frac{\Theta_{\mathrm{up}}^{\frac{N}{2}+1}}{\alpha L^2\left[\Gamma(N)\right]^2\varphi_1^{\frac{N}{2}+1}} \times \\ \Delta\left[\xi^{\alpha N+2\alpha+2}, G_{1,5}^{4,1}\left(\frac{\Theta_{\mathrm{up}}}{\varphi_1}\xi^{2\alpha}\Big|_{\frac{N}{2}-1,-1-\frac{N}{2},\frac{N}{2}-1,-\frac{N}{2},\varphi_2}^{-\frac{N}{2}-\frac{1}{\alpha}}\right)\right]\Bigg\}, \end{aligned} \tag{14}$$

where $\varphi_1 = \frac{\eta\rho P_t K\beta}{(1-\beta)\sigma_{\mathrm{up}}^2 d_{\mathrm{SR}}^{2\alpha}}$, $\varphi_2 = -\left(\frac{N}{2}+\frac{1}{\alpha}+1\right)$, Ξ is a large positive integer that determines the accuracy of the result and $G_{m,n}^{p,q}\left[x\big|_{b_1,\ldots,b_q}^{a_1,\ldots,a_p}\right]$ denotes the Meijer's G-function,.

Proof: Please refer to Appendix A. ■

Next, to obtain the uplink outage probability of the k-th IoT device in the optimal phase shift mode, one has the following lemma. Note that in the optimal phase shift mode, the phase shifts of the RIS are aligned with the k-th IoT device, but may not align with other IoT devices.

Lemma 2. Based on (12) and (13), if the phase shifts of the RIS are just aligned to the k-th IoT device, the expression of uplink outage probability can be given by

$$\begin{aligned} P_{\mathrm{up},k}^{\mathrm{O}} = \sum_{K=1}^{\Xi}\frac{\mu^K e^{-\mu}}{K!}\frac{\Theta_{\mathrm{up}}^{\zeta+1}}{\alpha L^2[\Gamma(\zeta)]^2\theta^{2\zeta+2}\varphi_1^{\zeta+1}}\times \\ \Delta\left[\xi^{2(\alpha\zeta+\alpha+1)}, G_{2,4}^{2,2}\left(\frac{\Theta_{\mathrm{up}}\xi^{2\alpha}}{\varphi_1\theta^2}\Big|_{-1,-1,-\zeta-1,-\zeta-\frac{1}{\alpha}-1}^{-\zeta,-\zeta-\frac{1}{\alpha}}\right)\right]. \end{aligned} \tag{15}$$

Proof: Please refer to Appendix B. ■

Note that a larger value of $P_{\mathrm{up,k}}$ indicates that a higher transmit power of the BS or more elements of the RIS are required. In addition, increasing the proportion coefficient ρ of PS or decreasing the time allocation coefficient β can also reduce the uplink outage probability of the whole system. However, this would lead to diminished performance in the downlink information transmission. As a result, there is a trade-off between the uplink and downlink transmission.

B. The average uplink data size of the k-th IoT device

Based on (10) and considering the Poisson distribution of the number of IoT devices, the average uplink data size of the k-th IoT device is given by

$$C_{\mathrm{up},k} = \sum_{K=1}^{\Xi}\frac{\mu^K e^{-\mu}(1-\beta)\tau_c}{K^2(K-1)!}\mathbb{E}[\log_2\left(1+\gamma_{\mathrm{up},k}\right)]. \tag{16}$$

where Ξ is a large positive integer that determines the accuracy of the result. Subsequently, we can establish the following lemma.

Lemma 3. The closed-form expression of average uplink data size for the k-th IoT device in the random phase shift model is given by

$$\begin{aligned} C_{\mathrm{up},k}^{\mathrm{R}} = \sum_{K=1}^{\Xi}\frac{\mu^K e^{-\mu}(1-\beta)\tau_c}{K^2(K-1)!\alpha L^2\left[\Gamma(N)\right]^2\ln 2} \times \\ \Delta\left[\xi^2, G_{2,6}^{5,2}\left(\frac{\xi^{2\alpha}}{\varphi_1}\Big|_{N,0,N,1,0,-\frac{1}{\alpha}}^{1-\frac{1}{\alpha},0}\right)\right]. \end{aligned} \tag{17}$$

Proof: Please refer to Appendix C. ■

Lemma 4. If the phase shifts of the RIS are just aligned to the k-th IoT device, an upper bound of average uplink data size for the k-th IoT device is derived as

$$\begin{aligned} C_{\mathrm{dl},k}^{\mathrm{O}} \approx \sum_{K=1}^{\Xi}\frac{\mu^K e^{-\mu}(1-\beta)\tau_c}{K^2(K-1)!} \times \\ \log_2\left(1+\frac{\varphi_1\zeta^2\theta^2\left(d_{\min}^{2-2\alpha}-d_{\max}^{2-2\alpha}\right)}{(\alpha-1)L^2}\right). \end{aligned} \tag{18}$$

Proof: Please refer to Appendix D. ■

IV. Extension to Rician fading channel and multi-antenna scenarios

A. Rician fading channel

In this subsection, the Rician fading channel model is studied. Given the traditional high-altitude deployment of both the RIS and BS, we assume that this is a line-of-sight (LoS) path between the RIS and BS. Accordingly, the channels from the RIS to the BS can be modeled by $\mathbf{g}_{\mathrm{dl}} = [g_{\mathrm{dl},1},\ldots,g_{\mathrm{dl},N}]^{\mathrm{H}}$, where $|g_{\mathrm{dl},n}| = 1$, $n \in \{1,\ldots,N\}$ [16].

Due to a large number of reflecting and scattering components from trees and stones surrounding IoT devices, the link between IoT devices and the RIS may experience both LoS and non-LoS (NLoS) fading. Therefore, the channel $\mathbf{h}_{\mathrm{dl},k}$ can be given by

$$\mathbf{h}_{\mathrm{dl},k} = \sqrt{\frac{\kappa}{1+\kappa}}\bar{\mathbf{h}}_{\mathrm{dl},k} + \sqrt{\frac{1}{1+\kappa}}\tilde{\mathbf{h}}_{\mathrm{dl},k} \tag{19}$$

where $\kappa \geq 0$ is the Rician factor, $\bar{\mathbf{h}}_{\mathrm{dl},k}$ denotes the LoS component and $\tilde{\mathbf{h}}_{\mathrm{dl},k}$ represents the NLoS component of $\mathbf{h}_{\mathrm{dl},k}$. Specifically, one has $\left|\left[\bar{\mathbf{h}}_{\mathrm{dl},k}\right]_n\right| = 1$ and $\left[\tilde{\mathbf{h}}_{\mathrm{dl},k}\right]_n \sim \mathcal{CN}(0,1)$, $n \in \{1,\ldots,N\}$. Now, for further derivation, we first determine the statistical characteristics of $\Lambda_{\mathrm{dl},k} = |\mathbf{g}_{\mathrm{dl}}^{\mathrm{H}}\mathbf{\Phi}_{\mathrm{dl}}\mathbf{h}_{\mathrm{dl},k}|^2$ under the Rician channel.

In the random phase shift model, the phase shift of each element of the RIS is randomly selected, i.e., $\phi_{\mathrm{dl},n} \sim \mathcal{U}(-\pi,\pi)$. Therefore, one has the following lemma.

Lemma 5. For the random phase shift model, the PDF and CDF of $\Lambda_{\mathrm{dl},k}^{\mathrm{R}}$ can be respectively derived as

$$f_{\Lambda_{\mathrm{up},k}^{\mathrm{R}}}(x)=\frac{1}{N}e^{-\frac{x}{N}} \qquad \text{and} \qquad F_{\Lambda_{\mathrm{up},k}^{\mathrm{R}}}(x)=1-e^{-\frac{x}{N}}. \tag{20}$$

Proof: Let $\mathbf{f}_k=\mathbf{g}_{\mathrm{dl}}^{\mathrm{H}}\mathbf{\Phi}_{\mathrm{dl}}\mathbf{h}_{\mathrm{dl},k}$, one has

$$\begin{aligned}\mathbf{f}_k&=\mathbf{g}_{\mathrm{dl}}^{\mathrm{H}}\mathbf{\Phi}_{\mathrm{dl}}\mathbf{h}_{\mathrm{dl},k}\\&=\sqrt{\frac{\kappa}{1+\kappa}}\mathbf{g}_{\mathrm{dl}}^{\mathrm{H}}\mathbf{\Phi}_{\mathrm{dl}}\bar{\mathbf{h}}_{\mathrm{dl},k}+\sqrt{\frac{1}{1+\kappa}}\mathbf{g}_{\mathrm{dl}}^{\mathrm{H}}\mathbf{\Phi}_{\mathrm{dl}}\tilde{\mathbf{h}}_{\mathrm{dl},k}\\&\sim\sqrt{\frac{\kappa}{1+\kappa}}\left[e^{j\left(\psi_1^{\mathrm{g}}+\psi_1^{\mathrm{h}}+\phi_1\right)},...,e^{j\left(\psi_N^{\mathrm{g}}+\psi_N^{\mathrm{h}}+\phi_N\right)}\right]^{\mathrm{T}}\\&\quad+\sqrt{\frac{1}{1+\kappa}}\mathcal{CN}(\mathbf{0},\mathbf{I}_N),\end{aligned} \tag{21}$$

where $\psi_n^{\mathrm{g}}=\arg\left(g_{\mathrm{up},n}\right)$ and $\psi_n^{\mathrm{h}}=\arg\left(h_{\mathrm{dl},k,n}\right)$.

Then, $\Lambda_{\mathrm{dl},k}^{\mathrm{R}}$ can be rewritten as

$$\Lambda_{\mathrm{dl},k}^{\mathrm{R}}=|\mathbf{g}_{\mathrm{dl}}^{\mathrm{H}}\mathbf{\Phi}_{\mathrm{dl}}\mathbf{h}_{\mathrm{dl},k}|^2=|\mathbf{1}_N^{\mathrm{T}}\mathbf{f}_k|^2=\Re\left(\mathbf{1}_N^{\mathrm{T}}\mathbf{f}_k\right)^2+\Im\left(\mathbf{1}_N^{\mathrm{T}}\mathbf{f}_k\right)^2. \tag{22}$$

where $\mathbf{1}_N$ represents a column vector with all one. Specifically, one has

$$\begin{aligned}\Re\left(\mathbf{1}_N^{\mathrm{T}}\mathbf{f}_k\right)&=\sum_{n=1}^{N}\Re\left\{\sqrt{\frac{\kappa}{1+\kappa}}e^{j\left(\psi_n^{\mathrm{g}}+\psi_n^{\mathrm{h}}+\phi_n\right)}\right.\\&\left.\quad+\sqrt{\frac{1}{1+\kappa}}\left[\mathcal{CN}\left(\mathbf{0},\mathbf{I}_N\right)\right]_n\right\}\sim\mathcal{CN}\left(0,\frac{N}{2}\right).\end{aligned} \tag{23}$$

Similarly, one has

$$\Im\left(\mathbf{1}_N^{\mathrm{T}}\mathbf{f}_k\right)\sim\mathcal{CN}\left(0,\frac{N}{2}\right). \tag{24}$$

Note that $\Re\left(\mathbf{1}_N^{\mathrm{T}}\mathbf{f}_k\right)$ in (23) and $\Im\left(\mathbf{1}_N^{\mathrm{T}}\mathbf{f}_k\right)$ in (24) are independent and identically distributed zero mean random variables with the same variance, thus $\Lambda_{\mathrm{dl},k}^{\mathrm{R}}$ should follow the chi-square distribution with two degrees of freedom, i.e., $\Lambda_{\mathrm{dl},k}^{\mathrm{R}}\sim\mathcal{X}^2(2,\frac{N}{2})$. As a special case, $\Lambda_{\mathrm{dl},k}^{\mathrm{R}}$ can be represented as an exponential distribution with parameter N. Therefore, (20) is obtained. ■

Corollary 1. For the optimal phase shift model, the PDF and CDF of $\Lambda_{\mathrm{dl},k}^{\mathrm{O}}$ can be respectively written as

$$\begin{aligned}f_{\Lambda_{\mathrm{up},k}^{\mathrm{O}}}(x)&=\frac{1}{2\sigma^2}e^{-\frac{s^2+x}{2\sigma^2}}I_0\left(\frac{s\sqrt{x}}{\sigma^2}\right),\\F_{\Lambda_{\mathrm{up},k}^{\mathrm{O}}}(x)&=1-Q_1\left(\frac{s}{\sigma},\frac{\sqrt{x}}{\sigma}\right),\end{aligned} \tag{25}$$

where $s=\sqrt{\frac{\kappa}{1+\kappa}}N$, $\sigma^2=\frac{N}{2(1+\kappa)}$, $I_0(\cdot)$ represents the modified Bessel function of the first kind with order zero and $Q_1(\cdot,\cdot)$ denotes the first-order Marcum Q-function.

Proof: For this case, the phase shift of the RIS are just aligned to the k-th IoT device, i.e., $\phi_{\mathrm{up},n}=-\arg\left(h_{\mathrm{up},k,n}\right)-\arg\left(g_{\mathrm{up},n}\right)$. Therefore, $\mathbf{f}_k$ in (21) can be rewritten as

$$\begin{aligned}\mathbf{f}_k&=\mathbf{g}_{\mathrm{dl}}^{\mathrm{H}}\mathbf{\Phi}_{\mathrm{dl}}\mathbf{h}_{\mathrm{dl},k}\\&\sim\sqrt{\frac{\kappa}{1+\kappa}}\left[1,1,...,1\right]^{\mathrm{T}}+\sqrt{\frac{1}{1+\kappa}}\mathcal{CN}(\mathbf{0},\mathbf{I}_N).\end{aligned} \tag{26}$$

As a result, $\Re\left(\mathbf{1}_N^{\mathrm{T}}\mathbf{f}_k\right)$ and $\Im\left(\mathbf{1}_N^{\mathrm{T}}\mathbf{f}_k\right)$ in (22) are respectively redefined as

$$\begin{aligned}\Re\left(\mathbf{1}_N^{\mathrm{T}}\mathbf{f}_k\right)&=\sum_{n=1}^{N}\Re\left\{\sqrt{\frac{\kappa}{1+\kappa}}+\sqrt{\frac{1}{1+\kappa}}\left[\mathcal{CN}\left(\mathbf{0},\mathbf{I}_N\right)\right]_n\right\}\\&\sim\mathcal{CN}\left(\sqrt{\frac{\kappa}{1+\kappa}}N,\frac{N}{2(\kappa+1)}\right)\end{aligned} \tag{27}$$

and

$$\Im\left(\mathbf{1}_N^{\mathrm{T}}\mathbf{f}_k\right)\sim\mathcal{CN}\left(0,\frac{N}{2(\kappa+1)}\right). \tag{28}$$

Since $\Re\left(\mathbf{1}_N^{\mathrm{T}}\mathbf{f}_k\right)$ in (27) and $\Im\left(\mathbf{1}_N^{\mathrm{T}}\mathbf{f}_k\right)$ in (28) have the same variance but different mean values, $\Lambda_{\mathrm{dl},k}^{\mathrm{O}}$ should follow the non-central chi-square distribution with two degrees of freedom, i.e., $\Lambda_{\mathrm{dl},k}^{\mathrm{O}}\sim\mathcal{X}^2\left(2,\sqrt{\frac{\kappa}{1+\kappa}}N,\frac{N}{2(\kappa+1)}\right)$. According to the statistical characteristics of the non-central chi-square distribution, (25) is obtained. ■

Next, we analyze the system performance under the Rician channel model.

Lemma 6. Based on (13) and (20), for the Rician fading channel, the closed-form expression of uplink outage probability for the k-th IoT device in the random phase shift model can be expressed as

$$\begin{aligned}P_{\mathrm{up},k}^{\mathrm{R}}=\sum_{K=1}^{\Xi}\frac{\mu^K e^{-\mu}}{K!}&\left\{1-\frac{\sqrt{\Theta_{\mathrm{up}}}}{\alpha NL^2\sqrt{\varphi_1}}\times\right.\\&\left.\Delta\left[\xi^{\alpha+2},G_{1,3}^{2,1}\left(\frac{\Theta_{\mathrm{up}}\xi^{2\alpha}}{N^2\varphi_1}\left|{}_{\frac{1}{2},-\frac{1}{2},-\frac{1}{\alpha}-\frac{1}{2}}^{\frac{1}{2}-\frac{1}{\alpha}}\right.\right)\right]\right\}.\end{aligned} \tag{29}$$

Proof: Please refer to Appendix E. ■

Lemma 7. Based on (13) and (25), if the phase shift of the RIS are just aligned to the k-th IoT device, the exact expression of uplink outage probability can be derived as

$$\begin{aligned}P_{\mathrm{up},k}^{\mathrm{O}}=\sum_{K=1}^{\Xi}\frac{\mu^K e^{-\mu}}{K!}&\left\{\sqrt{2}\sigma s^{-1}\exp\left(-\frac{s^2}{4\sigma^2}\right)M_{-\frac{1}{2},0}\left(\frac{s^2}{2\sigma^2}\right)\right.\\&-\frac{1}{L^2\sigma^2}\int_0^{\infty}\int_{d_{\min}}^{d_{\max}}ye^{-\frac{s^2+x}{2\sigma^2}}I_0\left(\frac{s\sqrt{x}}{\sigma^2}\right)\times\\&\left.Q_1\left(\frac{s}{\sqrt{\sigma^2}},\frac{\sqrt{\Theta_{\mathrm{up}}}y^{\alpha}}{\sqrt{\varphi_1\sigma^2x}}\right)\mathrm{d}y\mathrm{d}x\right\},\end{aligned} \tag{30}$$

where $M_{a,b}(z)$ denotes the Whittaker function.

Proof: Please refer to Appendix F. ■

Unfortunately, in (30), we can not obtain the closed-form of the integral due to its complexity. Similar to Lemma 2, we approximate $\Lambda_{\mathrm{dl},k}^{\mathrm{O}}$ as a Gamma random variable to obtain a traceable result. Therefore, one has the following corollary.

Corollary 2. For the optimal phase shift model, we approximate the uplink outage probability of the k-th IoT device as

$$\begin{aligned}P_{\mathrm{up},k}^{\mathrm{O}}\approx\sum_{K=1}^{\Xi}\frac{\mu^K e^{-\mu}}{K!}&\frac{\Theta_{\mathrm{up}}^{\zeta'+1}}{\alpha L^2[\Gamma(\zeta')]^2{\theta'}^{2\zeta'+2}\varphi_1^{\zeta'+1}}\times\\&\Delta\left[\xi^{2(\alpha\zeta'+\alpha+1)},G_{2,4}^{2,2}\left(\frac{\Theta_{\mathrm{up}}\xi^{2\alpha}}{\varphi_1{\theta'}^2}\left|{}_{-1,-1,-\zeta'-1,-\zeta'-\frac{1}{\alpha}-1}^{-\zeta',-\zeta'-\frac{1}{\alpha}}\right.\right)\right],\end{aligned} \tag{31}$$

where $\zeta'=\frac{(2\sigma^2+s^2)^2}{4\sigma^4+4\sigma^2s^2}$ and $\theta'=\frac{4\sigma^4+4\sigma^2s^2}{2\sigma^2+s^2}$.

Proof: According to (25), the mean and variance of $\Lambda^{\mathrm{O}}_{\mathrm{dl},k}$ can be expressed as $\mathbb{E}\left[\Lambda^{\mathrm{O}}_{\mathrm{dl},k}\right] = 2\sigma^2 + s^2$ and $Var(\Lambda^{\mathrm{O}}_{\mathrm{dl},k}) = 4\sigma^4 + 4\sigma^2 s^2$. The distribution of $\Lambda^{\mathrm{O}}_{\mathrm{dl},k}$ can be approximately matched to a Gamma random variable as $\Lambda^{\mathrm{O}}_{\mathrm{dl},k} \sim \Gamma\left(\zeta', \theta'\right)$, where $\zeta' = \frac{\left(\mathbb{E}\left[\Lambda^{\mathrm{O}}_{\mathrm{dl},k}\right]\right)^2}{Var\left(\Lambda^{\mathrm{O}}_{\mathrm{dl},k}\right)}$ and $\theta' = \frac{Var\left(\Lambda^{\mathrm{O}}_{\mathrm{dl},k}\right)}{\mathbb{E}\left[\Lambda^{\mathrm{O}}_{\mathrm{dl},k}\right]}$. ■

Lemma 8. The closed-form expression of average uplink data size for the k-th IoT device in the random phase shift model can be expressed as

$$C^{\mathrm{R}}_{\mathrm{up},k} = \sum_{K=1}^{\Xi} \frac{\mu^K e^{-\mu}(1-\beta)\tau_c}{K^2(K-1)!\alpha L^2 \ln 2} \times \Delta\left[\xi^2, G^{3,2}_{2,4}\left(\frac{\xi^{2\alpha}}{\varphi_1 N^2}\left|{}^{1-\frac{1}{\alpha},0}_{1,0,0,-\frac{1}{\alpha}}\right.\right)\right]. \tag{32}$$

Proof: The proof is similar to Appendix D, which is omitted for simplicity. ■

Furthermore, in the optimal phase shift, it is difficult to derive an exact expression of average uplink data size for the k-th IoT device. Therefore, similar to Lemma 4, an upper bound of the average uplink data size is derived by exploit the Jensen's inequality. One has the following lemma.

Lemma 9. If the phase shift of the RIS are just aligned to the k-th IoT device, an upper bound of average uplink data size for the k-th IoT device can be approximated as

$$C^{\mathrm{O}}_{\mathrm{dl},k} \approx \sum_{K=1}^{\Xi} \frac{\mu^K e^{-\mu}(1-\beta)\tau_c}{K^2(K-1)!} \times \log_2\left(1 + \frac{\varphi_1\left(N+\kappa N^2\right)^2\left(d_{\min}^{2-2\alpha} - d_{\max}^{2-2\alpha}\right)}{(1+\kappa)^2(\alpha-1)L^2}\right). \tag{33}$$

Proof: The proof is similar to Appendix D except that the expectation of $\Lambda^{\mathrm{O}}_{\mathrm{up},k}$ is given by $\mathbb{E}\left[\Lambda^{\mathrm{O}}_{\mathrm{dl},k}\right] = 2\sigma^2 + s^2 = \frac{N+\kappa N^2}{1+\kappa}$, where σ^2 and s are defined in (25). To this end, the proof is omitted for simplicity. ■

B. Multi-antenna mounted at the BS

In this subsection, the case where the BS is equipped with multiple antennas is discussed. Specifically, we assume that the BS is equipped with $M(M>1)$ antennas arranged in the form of uniform linear array (ULA) and the RIS is comprised with N ($N = N_x \times N_y$) reflecting elements arranged in the form of uniform planar array (UPA) [37]. In this case, based on the assumption of LoS and Rician fading channel in Section IV-A, the downlink and uplink channel matrices between the BS and the RIS are denoted as $\mathbf{G}_{\mathrm{dl}} \in \mathbb{C}^{N\times M}$ and $\mathbf{G}_{\mathrm{up}} \in \mathbb{C}^{M\times N}$, respectively. Then, the received signal at the k-th IoT device in (4) can be rewritten as

$$y_{\mathrm{dl},k} = \sqrt{d_{\mathrm{SR}}^{-\alpha} d_k^{-\alpha}}\mathbf{h}^{\mathrm{H}}_{\mathrm{dl},k}\mathbf{\Phi}_{\mathrm{dl}}\mathbf{G}_{\mathrm{dl}}\mathbf{w}x_{\mathrm{dl}} + \mathbf{w}_{\mathrm{dl},k}, \tag{34}$$

where $\mathbf{w}$ is the precoding vector. Then, one can have $\Omega_{\mathrm{dl},k} = \left|\mathbf{h}^{\mathrm{H}}_{\mathrm{dl},k}\mathbf{\Phi}_{\mathrm{dl}}\mathbf{G}_{\mathrm{dl}}\mathbf{w}\right|^2 = \left|\sum_{j=1}^{N}\mathcal{F}_j\left[\mathbf{h}_{\mathrm{dl},k}\right]_j\left[\mathbf{\Phi}_{\mathrm{dl}}\right]_{j,j}\right|^2$, where $\mathcal{F}_j = \left[\mathbf{G}_{\mathrm{dl}}\right]_{j,:}\mathbf{w}$ denotes the signal received by the j-th RIS element and $\left[\mathbf{G}_{\mathrm{dl}}\right]_{j,:}$ denotes the j-th line of matrix $\mathbf{G}_{\mathrm{dl}}$. Next, for analysis tractability and low-complexity design, the maximum-ratio transmission (MRT) precoding is applied, i.e., $\mathbf{w}_{\mathrm{MRT}} = \sqrt{P_{\mathrm{T}}}\frac{\alpha_{G,t}(z_G)}{\|\alpha_{G,t}(z_G)\|}$, where $\alpha_{G,t}(z_G) = \frac{1}{\sqrt{M}}\left[1, e^{\mathbb{i}z_G}, \cdots, e^{(M-1)\mathbb{i}z_G}\right]^T$ is the array response vector of the antenna, $z_G \triangleq \pi\sin\gamma_G$ and γ_G is the angle of departure (AoD) from the BS to the RIS [37]. Thus, one has $\Omega_{\mathrm{dl},k} = \left|\sum_{j=1}^{N}\mathcal{F}_j\left[\mathbf{h}_{\mathrm{dl},k}\right]_j\left[\mathbf{\Phi}_{\mathrm{dl}}\right]_{j,j}\right|^2 = P_{\mathrm{T}}M|\mathbf{1}_N^{\mathrm{T}}\mathbf{\Phi}_{\mathrm{dl}}\aleph\mathbf{h}_{\mathrm{dl},k}|^2 = P_{\mathrm{T}}M|\mathbf{1}_N^{\mathrm{T}}\mathbf{f}^{\S}_{\mathrm{dl},k}|^2 = P_{\mathrm{T}}\Lambda_{\mathrm{up},k}$, where $\mathbf{1}_N$ represents a column vector with all one, $\aleph = \mathrm{diag}\left(e^{\mathbb{i}\aleph_1}, \cdots, e^{\mathbb{i}\aleph_N}\right)$, $\aleph_n$ denotes the different phase incident on the j-th element and $\mathbf{f}^{\S}_{\mathrm{dl},k} = \mathbf{\Phi}_{\mathrm{dl}}\aleph\mathbf{h}_{\mathrm{dl},k}$. Based on the above analysis, one has the following lemma.

Lemma 10. Similar to Lemma 5 and Corollary 1, $\Lambda_{\mathrm{dl},k}$ can be represented as an exponential distribution and a non-central chi-square distribution with two degrees of freedom in the random phase shift and the optimal phase shift models, respectively. That is to say, $\Lambda^{\mathrm{R}}_{\mathrm{dl},k} \sim \mathrm{Exp}(MN)$ and $\Lambda^{\mathrm{O}}_{\mathrm{dl},k} \sim \mathcal{X}^2\left(2, \sqrt{\frac{M\kappa}{1+\kappa}}N, \frac{MN}{2(\kappa+1)}\right)$.

Proof: The proof is similar Lemma 5 and Corollary 1, which is omitted for simplicity. ■

Note that due to the channel reciprocity, $\Lambda_{\mathrm{up},k}$ and $\Lambda_{\mathrm{dl},k}$ are independent and identically distributed. Therefore, based on Lemma 10, the performance analysis results in the case of multi-antenna can be obtained using methods similar to those in Section III-A.

TABLE I: Table of Simulation Parameters.

Intensity λ (IoT devices/m^2)	0.1 [23]
Power splitting factor ρ	0.6
Downlink time factor β	0.6
Path-loss exponent α_1 for the Rayleigh channel	2.8
Path-loss exponent α_2 for the Rician channel	2.3
Vertical height of the RIS H (m)	5
The radius of the circular target area L (m)	5
The distance from the BS to the RIS $d_{\mathrm{SR}}(m)$	10
Decoding power consumption coefficient ϖ	10^{-10} [34]
Energy conversion efficiency of IoT device η	0.85
Noise power at the IoT device $\sigma^2_{\mathrm{dl},k}$ (dBm)	-74
Noise power at the BS σ^2_{up} (dBm)	-74
Transmission duration τ_c (sec)	1
Uplink transmission rate threshold $C_{\mathrm{up,th}}$ (bits)	0.1

V. Numerical results

In this section, we provided numerical results for the performance evaluation of the RIS-aided SWIPT system. Furthermore, we validated the effectiveness of the obtained results using Monte-Carlo simulations. For convenience, we summarize the main parameters adopted in Table I. Note that we set the path-loss exponent for the Rayleigh channel model to $\alpha = \alpha_1 = 2.8$, while the path loss index for the Rice channel model is set to $\alpha = \alpha_2 = 2.3$. Especially, we run 10^6 times of Monte-Carlo simulations in this paper.

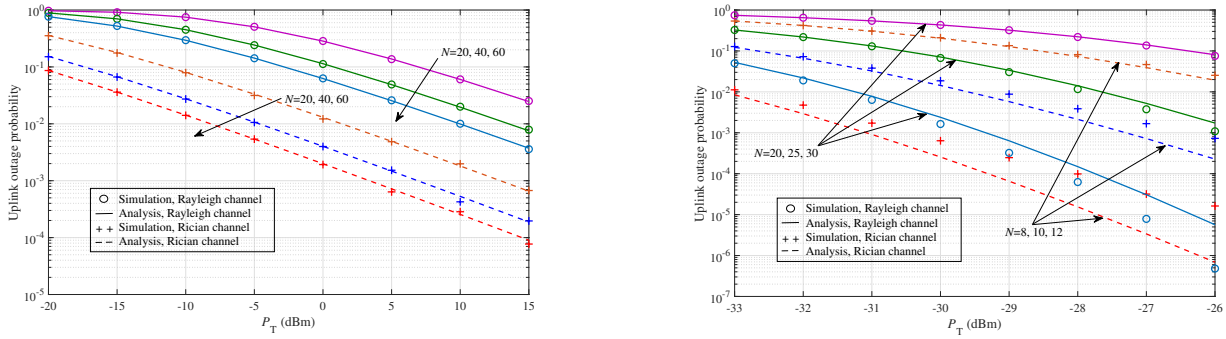

(a) Random phase shift (b) Optimal phase shift

Fig. 2: The uplink outage probability versus P_{T} for different values of N.

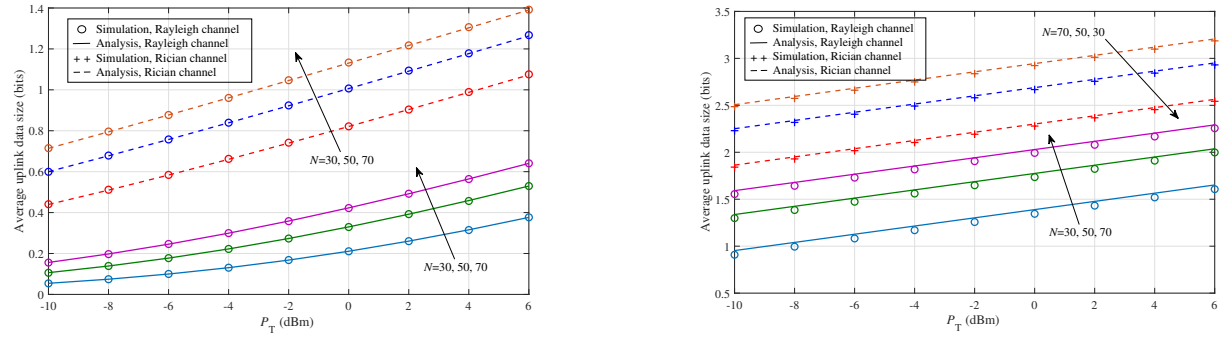

(a) Random phase shift (b) Optimal phase shift

Fig. 3: The average uplink data size versus P_{T} for different values of N.

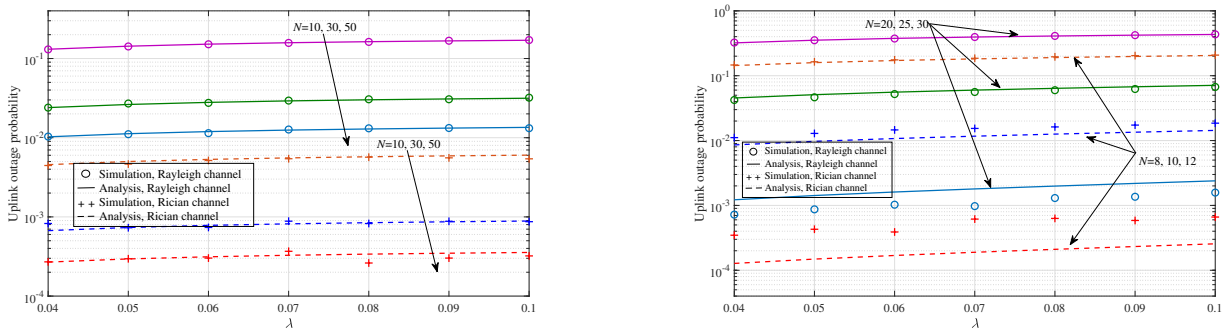

(a) Random phase shift (b) Optimal phase shift

Fig. 4: The uplink outage probability versus density λ for different values of N.

A. Rayleigh and Rician fading channels

Fig. 2 investigates the uplink outage probability versus P_{T} for different values of N under two phase shift and two fading channel models. We set the Rician coefficient κ to 1.5 in this figure. One can see that the uplink outage probability decrease with the increase of P_{T}, as expected. It is also observed that for any given P_{T}, lager values of N yields lower uplink outage probability. This is because increasing the transmit power of the BS or the number of N enables IoT devices to harvest more power in the downlink transmission phase to support them send more information in the uplink transmission phase. In addition, one can see that the uplink outage probability is more sensitive to the changes of N in the case of optimal phase shift than in the case of random phase shift. Specifically, under the optimal phase shift model, a smaller number of RIS elements are required to achieve the same outage performance as in the random phase shift model. Furthermore, compared to the random phase shift model, the small changes in the elements of the RIS under the optimal phase shift model lead to a significant decrease in outage probability. This phenomenon also appears in the simulation results of Fig. 4. This is because compared to the random phase shift model, higher channel

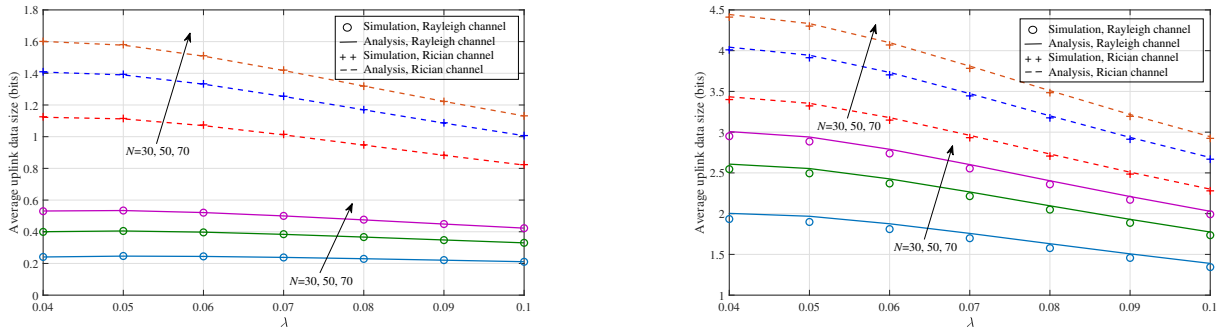

(a) Random phase shift

(b) Optimal phase shift

Fig. 5: The average uplink data size versus density λ for different values of N.

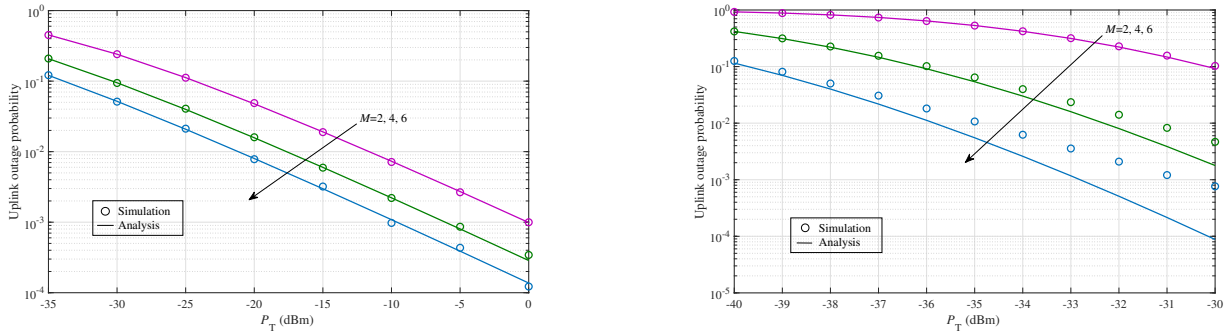

(a) Random phase shift

(b) Optimal phase shift

Fig. 6: The uplink outage probability versus P_{T} for different values of M.

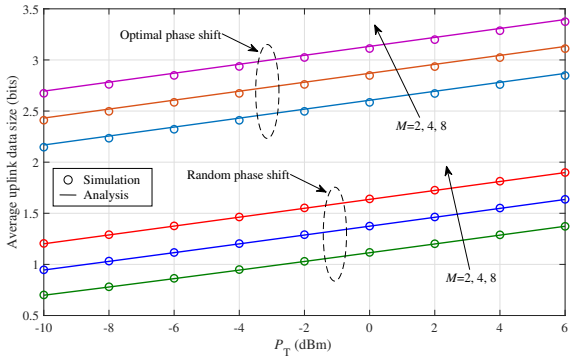

Fig. 7: The average uplink data size versus P_{T} for different values of M.

power gain can be obtained in the optimal phase shift model. Therefore, how to achieve the optimal phase shift should be the first priority in the actual deployment of the RIS.

In Fig. 3, we show the average uplink data size versus P_{T} with $\kappa = 10$ for $N \in \{30, 50, 70\}$ under the two phase shift and two fading channel models. It is easy to observe that increasing P_{T} or N always enhance the average uplink data size, which illustrates the benefits of increasing the transmit power of the BS or using more reflecting elements of the RIS. For fixed P_{T} and N, one can see that the average uplink data size in the optimal phase shift model and Rician channel are significantly better than those in the random phase shift model and Rayleigh channel condition. Similar to Fig. 2, this is also caused by the difference in channel gain generated by different phase shift models and channel conditions.

Fig. 4 illustrates the uplink outage probability versus λ for different values of N under two phase shift and two fading channel models. Specifically, we set the transmit power of the BS in Fig. 4(a) and 4(b) to 10 dBm and -30 dBm, respectively. The Rician factor κ is set to 1.5. One can see that the uplink outage probability increases with λ. This is because that there are more IoT devices when λ increase, resulting in less uplink transmission time for each IoT device. One can also observe from Fig. 4 that for a fixed λ, the uplink outage probability in both cases decreases with the increase of N due to the increased passive beamforming gain. Moreover, it is again observed that the uplink outage probability are more sensitive to the changes of λ in the case of optimal phase shift than in the case of random phase shift. In addition, similar to Fig. 2, one can see that under both the random phase shift and optimal phase shift models, the uplink outage probability under the Rician channel condition is lower than that of the Rayleigh channel.

In Fig. 5, we study the average uplink data size versus density λ with $P_{\mathrm{T}} = 0$ dBm and $\kappa = 10$ for $N \in \{30, 50, 70\}$ under two phase shift and two fading channel models. One can see that with the increase of λ, the average uplink data

size decreases. This observation can also be explained by the reason provided in Fig. 4. One can also see that increasing N yields higher average uplink data size. Particularly, it can be seen that the performance degradation of the average uplink data size occurs more rapidly in high-density regions compared to low-density regions.

B. Multi-Antenna case

Fig. 6 shows the uplink outage probability versus the transmit power of the BS for different values of M under the case of random phase shift and optimal phase shift in the Rician fading channel. Note that the the number of reflecting elements N in Fig. 6(a) and Fig. 6(b) are set to 40 and 20, respectively. We set the Rician factor κ to 1.5 in this case. It is observed that for any given P_{T}, lager values of M yields lower uplink outage probability. This means that increasing the quantity of antennas can substantially decrease the outage probability of the system under consideration. Furthermore, for the same case of phase shift, the gap between the curves in Fig. 6 decreases with the increase of M, which indicates that the extent of system performance improvement is gradually reduced.

Fig. 7 shows the average uplink data size versus P_{T} for $M \in \{2, 4, 8\}$. We set the number of RIS's elements to 30 and the Rician coefficient to 10 in this figure. It is easy to observe that increasing M always enhance the average uplink data size, which illustrates the benefits of using more antennas of the BS. One can also observe from Fig. 6 and Fig. 7 that the system performance in the optimal phase shift model is superior to that in the random phase shift model.

Again, in all these tests above, it can be seen that 'Analysis' curves are consistent with the 'Simulation' curves, indicating the usefulness and validity of our obtained results.

VI. Conclusion

In this paper, an RIS-assisted SWIPT system has been investigated by utilizing stochastic geometry tools. According to the transmission protocol considered, we have derived the closed-form expressions of the outage probability and the average data size for the k-th IoT device in the uplink transmission phase. Specifically, we considered not only the case of random phase shift, but also the case where the phase shift of the RIS are aligned to the k-th IoT device. Moreover, we also extended the Rayleigh channel to the Rician fading channel and multi-antenna scenarios. Finally, a large number of numerical results were provided to validate the effectiveness of our obtained results. For future work, we will discuss the performance of RIS-assisted SWIPT systems under more complex scenarios, e.g., the NOMA and compare them in detail with the existing TDMA scheme.

Appendix A
Proof of Lemma 1

Define $X_k = \Lambda^{\mathrm{R}}_{\mathrm{dl},k}\Lambda^{\mathrm{R}}_{\mathrm{up},k}$. To derive the closed-form expression of (13), we first identify the statistical features of X_k. Based on (11), the CDF of X_k can be expressed as

$$\begin{aligned}
&F_{X_k}(x)\\
&= \Pr\left\{\Lambda^{\mathrm{R}}_{\mathrm{dl},k}\Lambda^{\mathrm{R}}_{\mathrm{up},k} < x\right\} = \int_0^\infty F_{\Lambda^{\mathrm{R}}_{\mathrm{dl},k}}\left(\frac{x}{y}\right) f_{\Lambda^{\mathrm{R}}_{\mathrm{up},k}}(y)\mathrm{d}y\\
&= \int_0^\infty \left[1 - \frac{2}{\Gamma(N)}\left(\frac{x}{y}\right)^{\frac{N}{2}} K_N\left(2\sqrt{\frac{x}{y}}\right)\right] \times \\
&\qquad\qquad \frac{2}{\Gamma(N)} y^{\frac{N-1}{2}} K_{N-1}\left(2\sqrt{y}\right)\mathrm{d}y\\
&= 1 - \frac{4x^{\frac{N}{2}}}{\left[\Gamma(N)\right]^2}\int_0^\infty y^{-\frac{1}{2}} K_N\left(2\sqrt{\frac{x}{y}}\right) K_{N-1}\left(2\sqrt{y}\right)\mathrm{d}y\\
&\overset{(a)}{=} 1 - \frac{x^{\frac{N}{2}}}{\left[\Gamma(N)\right]^2}\int_0^\infty y^{-\frac{1}{2}} \times \\
&\qquad G^{0,2}_{2,0}\left(\frac{y}{x}\middle|^{1-\frac{N}{2},1+\frac{N}{2}}_{\cdot\quad\cdot}\right) G^{2,0}_{0,2}\left(y\middle|^{\cdot\quad\cdot}_{\frac{N-1}{2},-\frac{N-1}{2}}\right)\mathrm{d}y\\
&\overset{(b)}{=} 1 - \frac{x^{\frac{N}{2}+1}}{\left[\Gamma(N)\right]^2} G^{4,0}_{0,4}\left(x\middle|^{\cdot\quad\cdot\quad\cdot\quad\cdot}_{\frac{N}{2}-1,-1-\frac{N}{2},\frac{N}{2}-1,-\frac{N}{2}}\right),
\end{aligned} \tag{A.1}$$

where $G^{p,q}_{m,n}\left[x|^{a_1,\ldots,a_p}_{b_1,\ldots,b_q}\right]$ denotes the Meijer's G-function, (a) follows from [38, Eq. (8.4.23.1), Eq. (8.4.23.2)] and (b) is obtained by using [39, Eq. (9.31.5), Eq. (7.811.1)].

Then, (13) can be rewritten as

$$\begin{aligned}
&P^{\mathrm{R}}_{\mathrm{up},k} = \Pr\left\{X_k < \frac{\Theta_{\mathrm{up}} d_k^{2\alpha}}{\varphi_1}\right\} = \int_0^\infty F_{X_k}\left(\frac{\Theta_{\mathrm{up}} t^{2\alpha}}{\varphi_1}\right) f_{d_k}(t)\mathrm{d}t\\
&= \int_0^\infty \frac{2t}{L^2}\left[1 - \frac{\left(\Theta_{\mathrm{up}} t^{2\alpha}\right)^{\frac{N}{2}+1}}{\left[\Gamma(N)\right]^2 \varphi_1^{\frac{N}{2}+1}} \times \right.\\
&\qquad \left. G^{4,0}_{0,4}\left(\frac{\Theta_{\mathrm{up}} t^{2\alpha}}{\varphi_1}\middle|^{\cdot\quad\cdot\quad\cdot\quad\cdot}_{\frac{N}{2}-1,-1-\frac{N}{2},\frac{N}{2}-1,-\frac{N}{2}}\right)\right]\mathrm{d}t\\
&= 1 - \frac{2\Theta_{\mathrm{up}}^{\frac{N}{2}+1}}{L^2\left[\Gamma(N)\right]^2\varphi_1^{\frac{N}{2}+1}} \times \\
&\int_{d_{\min}}^{d_{\max}} t^{(N+2)\alpha+1} G^{4,0}_{0,4}\left(\frac{\Theta_{\mathrm{up}} t^{2\alpha}}{\varphi_1}\middle|^{\cdot\quad\cdot\quad\cdot\quad\cdot}_{\frac{N}{2}-1,-1-\frac{N}{2},\frac{N}{2}-1,-\frac{N}{2}}\right)\mathrm{d}t\\
&\overset{(a)}{=} 1 - \frac{\Theta_{\mathrm{up}}^{\frac{N}{2}+1}}{\alpha L^2\left[\Gamma(N)\right]^2\varphi_1^{\frac{N}{2}+1}} \times \\
&\left[d_{\max}^{\alpha N+2\alpha+2} G^{4,1}_{1,5}\left(\frac{\Theta_{\mathrm{up}} d_{\max}^{2\alpha}}{\varphi_1}\middle|^{-\frac{N}{2}-\frac{1}{\alpha}}_{\frac{N}{2}-1,-1-\frac{N}{2},\frac{N}{2}-1,-\frac{N}{2},\varphi_2}\right)\right.\\
&\left. - d_{\min}^{\alpha N+2\alpha+2} G^{4,1}_{1,5}\left(\frac{\Theta_{\mathrm{up}} d_{\min}^{2\alpha}}{\varphi_1}\middle|^{-\frac{N}{2}-\frac{1}{\alpha}}_{\frac{N}{2}-1,-1-\frac{N}{2},\frac{N}{2}-1,-\frac{N}{2},\varphi_2}\right)\right],
\end{aligned} \tag{A.2}$$

where $\varphi_1 = \frac{\eta\rho P_t\beta}{(1-\beta)\sigma^2_{\mathrm{up}} d^{2\alpha}_{\mathrm{SR}}}$, $\varphi_2 = -\left(\frac{N}{2} + \frac{1}{\alpha} + 1\right)$ and (a) follows from [38, Eq. (2.24.2.2)].

Finally, by taking the Poisson distributed number of IoT devices into consideration and further using $\Delta\left[\xi^{a_1}, G^{\cdot,\cdot}_{\cdot,\cdot}\left(b\xi^{a_2}\middle|^{\cdot,\cdot}_{\cdot,\cdot}\right)\right] \triangleq d^{a_1}_{\max} G^{\cdot,\cdot}_{\cdot,\cdot}\left(b d^{a_2}_{\max}\middle|^{\cdot,\cdot}_{\cdot,\cdot}\right) - d^{a_1}_{\min} G^{\cdot,\cdot}_{\cdot,\cdot}\left(b d^{a_2}_{\min}\middle|^{\cdot,\cdot}_{\cdot,\cdot}\right)$, (14) can be obtained.

Appendix B
Proof of Lemma 2

Define $Y_k = \Lambda^{\mathrm{O}}_{\mathrm{dl},k}\Lambda^{\mathrm{O}}_{\mathrm{up},k}$. In order to obtain the closed-form expression of (13) in the optimal phase shift model, we first

identify the statistical characteristics of Y_k. Based on (12), the CDF of Y_k can be given by

$$\begin{aligned}
F_{Y_k}(y) &= \Pr\left\{\Lambda^{\mathrm{O}}_{\mathrm{dl},k}\Lambda^{\mathrm{O}}_{\mathrm{up},k} < y\right\} \\
&= \int_0^\infty F_{\Lambda^{\mathrm{O}}_{\mathrm{dl},k}}\left(\frac{y}{z}\right) f_{\Lambda^{\mathrm{O}}_{\mathrm{up},k}}(z)\mathrm{d}z \\
&= \frac{1}{[\Gamma(\zeta)]^2\theta^\zeta}\int_0^\infty z^{\zeta-1}e^{-\frac{z}{\theta}}\Upsilon\left(\zeta,\frac{y}{\theta z}\right)\mathrm{d}z \\
&= \frac{1}{[\Gamma(\zeta)]^2\theta^\zeta}\int_0^\infty t^{-\zeta-1}e^{-\frac{1}{\theta t}}\Upsilon\left(\zeta,\frac{yt}{\theta}\right)\mathrm{d}t \\
&\overset{(a)}{=} \frac{1}{[\Gamma(\zeta)]^2\theta^\zeta}\int_0^\infty t^{-\zeta-1}G^{0,1}_{1,0}\left(\theta t\left|{}^{1}_{\cdot}\right.\right)G^{1,1}_{1,2}\left(\frac{yt}{\theta}\left|{}^{1}_{\zeta,0}\right.\right)\mathrm{d}t \\
&\overset{(b)}{=} \frac{y^{\zeta+1}}{[\Gamma(\zeta)]^2\theta^{2\zeta+2}}G^{2,1}_{1,3}\left(\frac{y}{\theta^2}\left|{}^{-\zeta}_{-1,-1,-\zeta-1}\right.\right),
\end{aligned} \tag{B.1}$$

where (a) is obtained by using [38, Eq. (8.4.3.2), Eq. (8.4.16.1)] and (b) follows from [39, Eq. (9.31.5), Eq. (7.811.1)].

Then, one can have

$$\begin{aligned}
P^{\mathrm{O}}_{\mathrm{up},k} &= \int_0^\infty F_{Y_k}\left(\frac{\Theta_{\mathrm{up}}t^{2\alpha}}{\varphi_1}\right)f_{d_k}(t)\mathrm{d}t \\
&= \frac{2\Theta_{\mathrm{up}}^{\zeta+1}}{L^2[\Gamma(\zeta)]^2\theta^{2\zeta+2}\varphi_1^{\zeta+1}} \times \\
&\quad \int_{d_{\min}}^{d_{\max}} t^{2\alpha\zeta+2\alpha+1}G^{2,1}_{1,3}\left(\frac{\Theta_{\mathrm{up}}t^{2\alpha}}{\varphi_1\theta^2}\left|{}^{-\zeta}_{-1,-1,-\zeta-1}\right.\right)\mathrm{d}t \\
&\overset{(a)}{=} \frac{\Theta_{\mathrm{up}}^{\zeta+1}}{\alpha L^2[\Gamma(\zeta)]^2\theta^{2\zeta+2}\varphi_1^{\zeta+1}} \times \\
&\left[d_{\max}^{2(\alpha\zeta+\alpha+1)}G^{2,2}_{2,4}\left(\frac{\Theta_{\mathrm{up}}d_{\max}^{2\alpha}}{\varphi_1\theta^2}\Big|{}^{-\zeta,-\zeta-\frac{1}{\alpha}}_{-1,-1,-\zeta-1,-\zeta-\frac{1}{\alpha}-1}\right)\right. \\
&\quad \left. - d_{\min}^{2(\alpha\zeta+\alpha+1)}G^{2,2}_{2,4}\left(\frac{\Theta_{\mathrm{up}}d_{\min}^{2\alpha}}{\varphi_1\theta^2}\Big|{}^{-\zeta,-\zeta-\frac{1}{\alpha}}_{-1,-1,-\zeta-1,-\zeta-\frac{1}{\alpha}-1}\right)\right],
\end{aligned} \tag{B.2}$$

where (a) follows from [38, Eq. (2.24.2.3)].

Finally, by taking the Poisson distributed number of IoT devices into consideration and defining $\Delta\left[\xi^{a_1},G^{\cdot,\cdot}_{\cdot,\cdot}\left(b\xi^{a_2}\left|{}^{\cdot,\cdot}_{\cdot,\cdot}\right.\right)\right] \triangleq d_{\max}^{a_1}G^{\cdot,\cdot}_{\cdot,\cdot}\left(bd_{\max}^{a_2}\left|{}^{\cdot,\cdot}_{\cdot,\cdot}\right.\right) - d_{\min}^{a_1}G^{\cdot,\cdot}_{\cdot,\cdot}\left(bd_{\min}^{a_2}\left|{}^{\cdot,\cdot}_{\cdot,\cdot}\right.\right)$, (15) can be obtained. The proof is completed.

Appendix C
Proof of Lemma 3

By exploiting the definition of average uplink data size, one has

$$C^{\mathrm{R}}_{\mathrm{up},k} = \sum_{K=1}^{\Xi}\frac{\mu^K e^{-\mu}(1-\beta)\tau_c}{K^2(K-1)!\ln 2}\int_0^\infty \frac{1-F_{\gamma^{\mathrm{R}}_{\mathrm{up},k}}(z)}{1+z}\mathrm{d}z. \tag{C.1}$$

To derive the closed-form expression of (C.1), we first derive the CDF of $\gamma^{\mathrm{R}}_{\mathrm{up},k}$. Similar to the derivation process of Lemma 1, the CDF of $\gamma^{\mathrm{R}}_{\mathrm{up},k}$ can be obtained as

$$\begin{aligned}
F_{\gamma^{\mathrm{R}}_{\mathrm{up},k}}(z) &= 1 - \frac{1}{\alpha L^2\left[\Gamma(N)\right]^2}\left(\frac{z}{\varphi_1}\right)^{\frac{N}{2}+1} \times \\
&\left[d_{\max}^{\alpha N+2\alpha+2}G^{4,1}_{1,5}\left(\frac{zd_{\max}^{2\alpha}}{\varphi_1}\left|{}^{-\frac{N}{2}-\frac{1}{\alpha}}_{\frac{N}{2}-1,-1-\frac{N}{2},\frac{N}{2}-1,-\frac{N}{2},-\left(\frac{N}{2}+\frac{1}{\alpha}+1\right)}\right.\right)\right. \\
&\quad \left. - d_{\min}^{\alpha N+2\alpha+2} \times \right. \\
&\qquad \left. G^{4,1}_{1,5}\left(\frac{zd_{\min}^{2\alpha}}{\varphi_1}\left|{}^{-\frac{N}{2}-\frac{1}{\alpha}}_{\frac{N}{2}-1,-1-\frac{N}{2},\frac{N}{2}-1,-\frac{N}{2},-\left(\frac{N}{2}+\frac{1}{\alpha}+1\right)}\right.\right)\right].
\end{aligned} \tag{C.2}$$

Then, substituting (C.2) into (C.1), one can have

$$\begin{aligned}
C^{\mathrm{R}}_{\mathrm{up},k} &= \sum_{K=1}^{\Xi}\frac{\mu^K e^{-\mu}(1-\beta)\tau_c}{K^2(K-1)!\alpha L^2\left[\Gamma(N)\right]^2\ln 2} \times \\
&\int_0^\infty \frac{d_{\max}^2}{1+z}\left(\frac{zd_{\max}^{2\alpha}}{\varphi_1}\right)^{\frac{N}{2}+1} \\
&\quad G^{4,1}_{1,5}\left(\frac{zd_{\max}^{2\alpha}}{\varphi_1}\left|{}^{-\frac{N}{2}-\frac{1}{\alpha}}_{\frac{N}{2}-1,-1-\frac{N}{2},\frac{N}{2}-1,-\frac{N}{2},-\left(\frac{N}{2}+\frac{1}{\alpha}+1\right)}\right.\right) \\
&- \frac{d_{\min}^2}{1+z}\left(\frac{zd_{\min}^{2\alpha}}{\varphi_1}\right)^{\frac{N}{2}+1} \\
&\quad G^{4,1}_{1,5}\left(\frac{zd_{\min}^{2\alpha}}{\varphi_1}\left|{}^{-\frac{N}{2}-\frac{1}{\alpha}}_{\frac{N}{2}-1,-1-\frac{N}{2},\frac{N}{2}-1,-\frac{N}{2},-\left(\frac{N}{2}+\frac{1}{\alpha}+1\right)}\right.\right)\mathrm{d}z \\
&= \sum_{K=1}^{\Xi}\frac{\mu^K e^{-\mu}(1-\beta)\tau_c}{K^2(K-1)!\alpha L^2\left[\Gamma(N)\right]^2\ln 2} \times \\
&\quad \left[d_{\max}^2 G^{5,2}_{2,6}\left(\frac{d_{\max}^{2\alpha}}{\varphi_1}\left|{}^{1-\frac{1}{\alpha},0}_{N,0,N,1,0,-\frac{1}{\alpha}}\right.\right)\right. \\
&\quad \left. - d_{\min}^2 G^{5,2}_{2,6}\left(\frac{d_{\min}^{2\alpha}}{\varphi_1}\left|{}^{1-\frac{1}{\alpha},0}_{N,0,N,1,0,-\frac{1}{\alpha}}\right.\right)\right].
\end{aligned} \tag{C.3}$$

Then, (17) is obtained by using $\Delta\left[\xi^{a_1},G^{\cdot,\cdot}_{\cdot,\cdot}\left(b\xi^{a_2}\left|{}^{\cdot,\cdot}_{\cdot,\cdot}\right.\right)\right] \triangleq d_{\max}^{a_1}G^{\cdot,\cdot}_{\cdot,\cdot}\left(bd_{\max}^{a_2}\left|{}^{\cdot,\cdot}_{\cdot,\cdot}\right.\right) - d_{\min}^{a_1}G^{\cdot,\cdot}_{\cdot,\cdot}\left(bd_{\min}^{a_2}\left|{}^{\cdot,\cdot}_{\cdot,\cdot}\right.\right)$.

Appendix D
Proof of Lemma 4

By exploiting the definition of average uplink data size, (16) can be given by

$$C^{\mathrm{O}}_{\mathrm{up},k} = \sum_{K=1}^{\Xi}\frac{\mu^K e^{-\mu}(1-\beta)\tau_c}{K^2(K-1)!\ln 2}\int_0^\infty \frac{1-F_{\gamma^{\mathrm{O}}_{\mathrm{up},k}}(z)}{1+z}\mathrm{d}z. \tag{D.1}$$

In order to obtain the closed-form expression of (D.1), we first derive the CDF of $\gamma^{\mathrm{O}}_{\mathrm{up},k}$. Similar to the derivation process of Lemma 2, the CDF of $\gamma^{\mathrm{O}}_{\mathrm{up},k}$ can be obtained as

$$\begin{aligned}
F_{\gamma^{\mathrm{O}}_{\mathrm{up},k}}(z) &= \frac{z^{\zeta+1}}{\alpha L^2[\Gamma(\zeta)]^2\theta^{2\zeta+2}\varphi_1^{\zeta+1}} \times \\
&\left[d_{\max}^{2(\alpha\zeta+\alpha+1)}G^{2,2}_{2,4}\left(\frac{zd_{\max}^{2\alpha}}{\theta^2\varphi_1}\Big|{}^{-\zeta,-\zeta-\frac{1}{\alpha}}_{-1,-1,-\zeta-1,-\zeta-\frac{1}{\alpha}-1}\right)\right. \\
&\quad \left. - d_{\min}^{2(\alpha\zeta+\alpha+1)}G^{2,2}_{2,4}\left(\frac{zd_{\min}^{2\alpha}}{\theta^2\varphi_1}\Big|{}^{-\zeta,-\zeta-\frac{1}{\alpha}}_{-1,-1,-\beta-1,-\zeta-\frac{1}{\alpha}-1}\right)\right].
\end{aligned} \tag{D.2}$$

Then, one has

$$C_{\mathrm{up},k}^{\mathrm{O}} = \sum_{K=1}^{\Xi} \frac{\mu^K e^{-\mu}(1-\beta)\tau_c}{K^2(K-1)!\ln 2} \times \int_0^{\infty} \frac{1}{1+z} \left\{ 1 - \frac{z^{\zeta+1}}{\alpha L^2 [\Gamma(\zeta)]^2 \theta^{2\zeta+2} \varphi_1^{\zeta+1}} \times \left[d_{\max}^{2(\alpha\zeta+\alpha+1)} G_{2,4}^{2,2}\left(\frac{z d_{\max}^{2\alpha}}{\theta^2 \varphi_1} \middle|_{-1,-1,-\zeta-1,-\zeta-\frac{1}{\alpha}-1}^{-\zeta,-\zeta-\frac{1}{\alpha}} \right) - d_{\min}^{2(\alpha\zeta+\alpha+1)} G_{2,4}^{2,2}\left(\frac{z d_{\min}^{2\alpha}}{\theta^2 \varphi_1} \middle|_{-1,-1,-\zeta-1,-\zeta-\frac{1}{\alpha}-1}^{-\zeta,-\zeta-\frac{1}{\alpha}} \right) \right] \right\} \mathrm{d}z. \tag{D.3}$$

Unfortunately, it is difficult to derive the exact expression for (D.3). Therefore, by exploiting the Jensen's inequality, an upper bound of (D.1) can be given by

$$C_{\mathrm{up},k}^{\mathrm{O}} \leq \overline{C_{\mathrm{up},k}^{\mathrm{O}}} = \sum_{K=1}^{\Xi} \frac{\mu^K e^{-\mu}(1-\beta)\tau_c}{K^2(K-1)!} \log_2\left(1 + \mathbb{E}[\gamma_{\mathrm{up},k}^{\mathrm{O}}]\right). \tag{D.4}$$

Then, due to $\Lambda_{\mathrm{dl},k}^{\mathrm{O}}$, $\Lambda_{\mathrm{up},k}^{\mathrm{O}}$ and $d_k^{-2\alpha}$ are independent of each other, $\mathbb{E}[\gamma_{\mathrm{up},k}^{\mathrm{O}}]$ can be given by

$$\begin{aligned} \mathbb{E}[\gamma_{\mathrm{up},k}^{\mathrm{O}}] &= \mathbb{E}\left[\varphi_1 \Lambda_{\mathrm{dl},k}^{\mathrm{O}} \Lambda_{\mathrm{up},k}^{\mathrm{O}} d_k^{-2\alpha}\right] \\ &= \varphi_1 \mathbb{E}\left[\Lambda_{\mathrm{dl},k}\right] \mathbb{E}\left[\Lambda_{\mathrm{up},k}\right] \mathbb{E}\left[d_k^{-2\alpha}\right]. \end{aligned} \tag{D.5}$$

Based on (3), $\mathbb{E}\left[d_k^{-2\alpha}\right]$ in (D.5) can be derived as $\mathbb{E}\left[d_k^{-2\alpha}\right] = \frac{1}{(\alpha-1)L^2}\left(d_{\min}^{2-2\alpha} - d_{\max}^{2-2\alpha}\right)$. In addition, based on (11) and following [39, Eq. (3.351.3)], one can have $\mathbb{E}\left[\Lambda_{\mathrm{dl},k}^{\mathrm{O}}\right] = \mathbb{E}\left[\Lambda_{\mathrm{up},k}^{\mathrm{O}}\right] = \theta\zeta$. As a result, one has

$$\mathbb{E}[\gamma_{\mathrm{up},k}^{\mathrm{O}}] = \frac{\varphi_1 \zeta^2 \theta^2 \left(d_{\min}^{2-2\alpha} - d_{\max}^{2-2\alpha}\right)}{(\alpha-1)L^2}. \tag{D.6}$$

Finally, substituting (D.6) into (D.4), (18) is obtained. Here, the proof is completed.

Appendix E
Proof of Lemma 5

Define $U_k = \Lambda_{\mathrm{dl},k}^{\mathrm{R}} \Lambda_{\mathrm{up},k}^{\mathrm{R}}$. To derive the closed-form expression of (13), we first determine the statistical features of U_k. Based on (20), the CDF of U_k can be expressed as

$$\begin{aligned} &F_{U_k}(u) \\ &= \Pr\left\{\Lambda_{\mathrm{dl},k}^{\mathrm{R}} \Lambda_{\mathrm{up},k}^{\mathrm{R}} < u\right\} = \int_0^{\infty} F_{\Lambda_{\mathrm{dl},k}^{\mathrm{R}}}\left(\frac{u}{y}\right) f_{\Lambda_{\mathrm{up},k}^{\mathrm{R}}}(y)\mathrm{d}y \\ &= \frac{1}{N}\int_0^{\infty} \left(1 - e^{-\frac{u}{Ny}}\right) e^{-\frac{y}{N}} \mathrm{d}y \\ &= 1 - \frac{1}{N}\int_0^{\infty} e^{-\frac{u}{Ny} - \frac{y}{N}} \mathrm{d}y \overset{(a)}{=} 1 - \frac{2\sqrt{u}}{N} K_1\left(\frac{2\sqrt{u}}{N}\right), \end{aligned} \tag{E.1}$$

where (a) follows from [39, 3.471.9].

Then, one has

$$\begin{aligned} P_{\mathrm{up},k}^{\mathrm{R}} &= \Pr\left\{U_k < \frac{\Theta_{\mathrm{up}} d_k^{2\alpha}}{\varphi_1}\right\} \\ &= \int_0^{\infty} F_{U_k}\left(\frac{\Theta_{\mathrm{up}} t^{2\alpha}}{\varphi_1}\right) f_{d_k}(t)\mathrm{d}t \\ &= \int_0^{\infty} \frac{2t}{L^2}\left[1 - \frac{2t^{\alpha}\sqrt{\Theta_{\mathrm{up}}}}{N\sqrt{\varphi_1}} K_1\left(\frac{2t^{\alpha}\sqrt{\Theta_{\mathrm{up}}}}{N\sqrt{\varphi_1}}\right)\right]\mathrm{d}t \\ &= 1 - \frac{4\sqrt{\Theta_{\mathrm{up}}}}{NL^2\sqrt{\varphi_1}} \int_{d_{\min}}^{d_{\max}} t^{\alpha+1} K_1\left(\frac{2t^{\alpha}\sqrt{\Theta_{\mathrm{up}}}}{N\sqrt{\varphi_1}}\right) \\ &\overset{(a)}{=} 1 - \frac{\sqrt{\Theta_{\mathrm{up}}}}{\alpha N L^2 \sqrt{\varphi_1}} \int_{d_{\min}^{2\alpha}}^{d_{\max}^{2\alpha}} x^{\frac{1}{\alpha}-\frac{1}{2}} G_{0,2}^{2,0}\left(\frac{\Theta_{\mathrm{up}} x}{\varphi_1 N^2} \middle|_{\frac{1}{2},-\frac{1}{2}}^{\cdot\ \cdot}\right)\mathrm{d}x \\ &\overset{(b)}{=} 1 - \frac{\sqrt{\Theta_{\mathrm{up}}}}{\alpha N L^2 \sqrt{\varphi_1}} \left[d_{\max}^{\alpha+2} G_{1,3}^{2,1}\left(\frac{\Theta_{\mathrm{up}} d_{\max}^{2\alpha}}{\varphi_1 N^2} \middle|_{\frac{1}{2},-\frac{1}{2},-\frac{1}{\alpha}-\frac{1}{2}}^{\frac{1}{2}-\frac{1}{\alpha}}\right) - d_{\min}^{\alpha+2} G_{1,3}^{2,1}\left(\frac{\Theta_{\mathrm{up}} d_{\min}^{2\alpha}}{\varphi_1 N^2} \middle|_{\frac{1}{2},-\frac{1}{2},-\frac{1}{\alpha}-\frac{1}{2}}^{\frac{1}{2}-\frac{1}{\alpha}}\right)\right], \end{aligned} \tag{E.2}$$

where (a) is obtained by using [38, Eq. (8.4.23.2)] and (b) follows from [38, Eq. (2.24.2.2)].

Finally, by taking the Poisson distributed number of IoT devices into consideration and further using $\Delta\left[\xi^{a_1}, G_{\cdot,\cdot}^{\cdot,\cdot}\left(b\xi^{a_2}\middle|_{\cdot,\cdot}^{\cdot,\cdot}\right)\right] \triangleq d_{\max}^{a_1} G_{\cdot,\cdot}^{\cdot,\cdot}\left(b d_{\max}^{a_2}\middle|_{\cdot,\cdot}^{\cdot,\cdot}\right) - d_{\min}^{a_1} G_{\cdot,\cdot}^{\cdot,\cdot}\left(b d_{\min}^{a_2}\middle|_{\cdot,\cdot}^{\cdot,\cdot}\right)$, (29) can be obtained.

Appendix F
Proof of Lemma 7

Define $V_k = \frac{\Lambda_{\mathrm{dl},k}^{\mathrm{O}}}{d_k^{2\alpha}}$. In order to obtain the closed-form expression of (13), we first identify the statistical characteristics of V_k. Based on (3) and (25), the CDF of V_k can be expressed as

$$\begin{aligned} F_{V_k}(v) &= \int_0^{\infty} F_{\Lambda_{\mathrm{dl},k}^{\mathrm{O}}}\left(v y^{2\alpha}\right) f_{d_k}(y)\mathrm{d}y \\ &= \frac{2}{L^2}\int_{d_{\min}}^{d_{\max}} y\left[1 - Q_1\left(\frac{s}{\sqrt{\sigma^2}}, \frac{\sqrt{v}y^{\alpha}}{\sqrt{\sigma^2}}\right)\right]\mathrm{d}y. \end{aligned} \tag{F.1}$$

Then, one can have

$$\begin{aligned} P_{\mathrm{up},k}^{\mathrm{O}} &= \int_0^{\infty} F_{V_k}\left(\frac{\Theta_{\mathrm{up}}}{\varphi_1 t}\right) f_{\Lambda_{\mathrm{up},k}^{\mathrm{O}}}(t)\mathrm{d}t \\ &= \underbrace{\frac{1}{2\sigma^2}\int_0^{\infty} e^{-\frac{s^2+t}{2\sigma^2}} I_0\left(\frac{s\sqrt{t}}{\sigma^2}\right)\mathrm{d}t}_{I_1} \\ &\quad - \frac{1}{L^2\sigma^2}\int_0^{\infty}\int_{d_{\min}}^{d_{\max}} y e^{-\frac{s^2+x}{2\sigma^2}} I_0\left(\frac{s\sqrt{x}}{\sigma^2}\right) \\ &\quad \times Q_1\left(\frac{s}{\sqrt{\sigma^2}}, \frac{\sqrt{\Theta_{\mathrm{up}}}y^{\alpha}}{\sqrt{\varphi_1\sigma^2 x}}\right)\mathrm{d}y\mathrm{d}x. \end{aligned} \tag{F.2}$$

By using [39, Eq. (6.614.3)], one can have

$$I_1 = \sqrt{2}\sigma s^{-1} \exp\left(-\frac{s^2}{4\sigma^2}\right) M_{-\frac{1}{2},0}\left(\frac{s^2}{2\sigma^2}\right), \tag{F.3}$$

where $M_{a,b}(z)$ denotes the Whittaker function.

Finally, by taking the Poisson distributed number of IoT devices into consideration and substituting (F.3) into (F.1), (30) can be obtained. The proof is completed.

REFERENCES

[1] H. Jiang, M. Mukherjee, J. Zhou, and J. Lloret, "Channel modeling and characteristics for 6G wireless communications," *IEEE Netw.*, vol. 35, no. 1, pp. 296–303, Jan./Feb. 2021.

[2] J. Hu, K. Yang, G. Wen, and L. Hanzo, "Integrated data and energy communication network: A comprehensive survey," *IEEE Commun. Surveys Tuts.*, vol. 20, no. 4, pp. 3169–3219, 4st Quart. 2018.

[3] T. D. Ponnimbaduge Perera, D. N. K. Jayakody, S. K. Sharma, S. Chatzinotas, and J. Li, "Simultaneous wireless information and power transfer (SWIPT): Recent advances and future challenges," *IEEE Commun. Surveys Tuts.*, vol. 20, no. 1, pp. 264–302, 1st Quart. 2018.

[4] N. Khalfet and I. Krikidis, "Information energy capacity region for SWIPT systems over Rayleigh-fading channels," *IEEE Trans. Commun.*, vol. 71, no. 3, pp. 1416–1429, Mar. 2023.

[5] K. W. Choi, S. I. Hwang, A. A. Aziz, H. H. Jang, J. S. Kim, D. S. Kang, and D. I. Kim, "Simultaneous wireless information and power transfer (SWIPT) for internet of things: Novel receiver design and experimental validation," *IEEE Internet Things J.*, vol. 7, no. 4, pp. 2996–3012, Apr. 2020.

[6] Y. Zhao, J. Hu, A. Xie, K. Yang, and K.-K. Wong, "Receive spatial modulation aided simultaneous wireless information and power transfer with finite alphabet," *IEEE Trans. Wireless Commun.*, vol. 19, no. 12, pp. 8039–8053, Dec. 2020.

[7] A. S. Parihar, P. Swami, and V. Bhatia, "On performance of SWIPT enabled PPP distributed cooperative NOMA networks using stochastic geometry," *IEEE Trans. Veh. Technol.*, vol. 71, no. 5, pp. 5639–5644, May 2022.

[8] I.-M. Kim, D. I. Kim, and J.-M. Kang, "Rate-energy tradeoff and decoding error probability-energy tradeoff for SWIPT in finite code length," *IEEE Trans. Wireless Commun.*, vol. 16, no. 12, pp. 8220–8234, Dec. 2017.

[9] C. Pan, H. Ren, K. Wang, J. F. Kolb, M. Elkashlan, M. Chen, M. Di Renzo, Y. Hao, J. Wang, A. L. Swindlehurst, X. You, and L. Hanzo, "Reconfigurable intelligent surfaces for 6G systems: Principles, applications, and research directions," *IEEE Commun. Mag.*, vol. 59, no. 6, pp. 14–20, Jun. 2021.

[10] Q. Wu and R. Zhang, "Towards smart and reconfigurable environment: Intelligent reflecting surface aided wireless network," *IEEE Commun. Mag.*, vol. 58, no. 1, pp. 106–112, Jan. 2020.

[11] Q.-U.-A. Nadeem, A. Zappone, and A. Chaaban, "Intelligent reflecting surface enabled random rotations scheme for the MISO broadcast channel," *IEEE Trans. Wireless Commun.*, vol. 20, no. 8, pp. 5226–5242, Aug. 2021.

[12] R. Hashemi, S. Ali, N. H. Mahmood, and M. Latva-aho, "Average rate and error probability analysis in short packet communications over RIS-aided URLLC systems," *IEEE Trans. Veh. Technol.*, vol. 70, no. 10, pp. 10 320–10 334, Oct. 2021.

[13] B. Zhang, K. Wang, K. Yang, and G. Zhang, "IRS-assisted short packet wireless energy transfer and communications," *IEEE Wireless Commun. Lett.*, vol. 11, no. 2, pp. 303–307, Feb. 2022.

[14] X. Liu, Y. Liu, and Y. Chen, "Machine learning empowered trajectory and passive beamforming design in UAV-RIS wireless networks," *IEEE J. Sel. Areas Commun.*, vol. 39, no. 7, pp. 2042–2055, Jul. 2021.

[15] Z. Huang, B. Zheng, and R. Zhang, "Transforming fading channel from fast to slow: Intelligent refracting surface aided high-mobility communication," *IEEE Trans. Wireless Commun.*, vol. 21, no. 7, pp. 4989–5003, Jul. 2022.

[16] Z. Shi, H. Wang, Y. Fu, X. Ye, G. Yang, and S. Ma, "Outage performance and AoI minimization of HARQ-IR-RIS aided IoT networks," *IEEE Trans. Commun*, vol. 71, no. 3, pp. 1740–1754, Mar. 2023.

[17] Z. Chen, J. Tang, X. Y. Zhang, D. K. C. So, S. Jin, and K.-K. Wong, "Hybrid evolutionary-based sparse channel estimation for IRS-assisted mmwave MIMO systems," *IEEE Trans. Wireless Commun.*, vol. 21, no. 3, pp. 1586–1601, Mar. 2022.

[18] T. Hou, Y. Liu, Z. Song, X. Sun, Y. Chen, and L. Hanzo, "Reconfigurable intelligent surface aided NOMA networks," *IEEE J. Sel. Areas Commun.*, vol. 38, no. 11, pp. 2575–2588, Nov. 2020.

[19] H. Wang, C. Liu, Z. Shi, Y. Fu, and R. Song, "Power minimization for uplink RIS-assisted CoMP-NOMA networks with GSIC," *IEEE Trans. Commun*, vol. 70, no. 7, pp. 4559–4573, Jul. 2022.

[20] A. Bansal, K. Singh, B. Clerckx, C.-P. Li, and M.-S. Alouini, "Rate-splitting multiple access for intelligent reflecting surface aided multi-user communications," *IEEE Trans. Veh. Technol.*, vol. 70, no. 9, pp. 9217–9229, Sep. 2021.

[21] Z. Yang, P. Xu, G. Chen, Y. Wu, and Z. Ding, "Performance analysis of IRS-assisted NOMA networks with randomly deployed users," *IEEE Syst. J.*, vol. 17, no. 2, pp. 1853–1864, Jun. 2023.

[22] T. Hou, Y. Liu, Z. Song, X. Sun, Y. Chen, and L. Hanzo, "MIMO assisted networks relying on intelligent reflective surfaces: A stochastic geometry based analysis," *IEEE Trans. Veh. Technol.*, vol. 71, no. 1, pp. 571–582, Jan. 2022.

[23] J. Lyu and R. Zhang, "Hybrid active/passive wireless network aided by intelligent reflecting surface: System modeling and performance analysis," *IEEE Trans. Wireless Commun.*, vol. 20, no. 11, pp. 7196–7212, Nov. 2021.

[24] B. Zhang, K. Yang, K. Wang, and G. Zhang, "Performance analysis of RIS-assisted wireless communications with energy harvesting," *IEEE Trans. Veh. Technol.*, vol. 72, no. 1, pp. 1325–1330, Jan. 2023.

[25] C. Pan, H. Ren, K. Wang, M. Elkashlan, A. Nallanathan, J. Wang, and L. Hanzo, "Intelligent reflecting surface aided MIMO broadcasting for simultaneous wireless information and power transfer," *IEEE J. Sel. Areas Commun.*, vol. 38, no. 8, pp. 1719–1734, Aug. 2020.

[26] Q. Wu and R. Zhang, "Joint active and passive beamforming optimization for intelligent reflecting surface assisted SWIPT under QoS constraints," *IEEE J. Sel. Areas Commun.*, vol. 38, no. 8, pp. 1735–1748, Aug. 2020.

[27] Z. Chen, J. Tang, N. Zhao, M. Liu, and D. K. C. So, "Hybrid beamforming with discrete phase shifts for RIS-assisted multiuser SWIPT system," *IEEE Wireless Commun. Lett.*, vol. 12, no. 1, pp. 104–108, Jan. 2023.

[28] S. Gong, Z. Yang, C. Xing, J. An, and L. Hanzo, "Beamforming optimization for intelligent reflecting surface-aided SWIPT IoT networks relying on discrete phase shifts," *IEEE Internet Things J.*, vol. 8, no. 10, pp. 8585–8602, May 2021.

[29] D. Xu, V. Jamali, X. Yu, D. W. K. Ng, and R. Schober, "Optimal resource allocation design for large IRS-assisted SWIPT systems: A scalable optimization framework," *IEEE Trans. Commun.*, vol. 70, no. 2, pp. 1423–1441, Feb. 2022.

[30] Z. Li, W. Chen, Q. Wu, K. Wang, and J. Li, "Joint beamforming design and power splitting optimization in IRS-assisted SWIPT NOMA networks," *IEEE Trans. Wireless Commun.*, vol. 21, no. 3, pp. 2019–2033, Mar. 2022.

[31] G. Chen, Q. Wu, W. Chen, D. W. K. Ng, and L. Hanzo, "IRS-aided wireless powered MEC systems: TDMA or NOMA for computation offloading?" *IEEE Trans. Wireless Commun.*, vol. 22, no. 2, pp. 1201–1218, Feb. 2023.

[32] L. Zhai, Y. Zou, J. Zhu, and H. Guo, "A stackelberg game approach for IRS-aided WPCN multicast systems," *IEEE Trans. Wireless Commun.*, vol. 21, no. 5, pp. 3249–3262, May 2022.

[33] G. Xiao, T. Yang, C. Huang, X. Wu, H. Feng, and B. Hu, "Average rate approximation and maximization for RIS-assisted multi-user MISO system," *IEEE Wireless Commun. Lett.*, vol. 11, no. 1, pp. 173–177, Jan. 2022.

[34] M. Abedi, H. Masoumi, and M. J. Emadi, "Power splitting-based SWIPT systems with decoding cost," *IEEE Wireless Commun. Lett.*, vol. 8, no. 2, pp. 432–435, Apr. 2019.

[35] X. Yue and Y. Liu, "Performance analysis of intelligent reflecting surface assisted NOMA networks," *IEEE Trans. Wireless Commun.*, vol. 21, no. 4, pp. 2623–2636, Apr. 2022.

[36] H. Ren, K. Wang, and C. Pan, "Intelligent reflecting surface-aided URLLC in a factory automation scenario," *IEEE Trans. Commun.*, vol. 70, no. 1, pp. 707–723, Jan. 2022.

[37] C. Luo, J. Hu, L. Xiang, K. Yang, and K.-K. Wong, "Massive wireless energy transfer without channel state information via imperfect intelligent reflecting surfaces," 2023. [Online]. Available: https://api.semanticscholar.org/CorpusID:265212761.

[38] A. P. Prudnikov, Y. A. Brychkov, and O. I. Marichev, *Integrals and series: Vol. 3: More special functions*. New York: CRC Press, 1992.

[39] I. S. Gradshteyn and I. M. Ryzhik, *Table of Integrals, Series, and Products,* 7th. San Diego, CA: Academic Press, 2007.

Bingxin Zhang received his M.S. degree from the School of Information and Control Engineering of China University of Mining and Technology, Xuzhou, China, in 2020. He is currently pursuing the Ph.D. degree in the School of Information and Communication Engineering, University of Electronic Science and Technology of China, Chengdu, China. His research interests include ultra-reliable low-latency communications (URLLC), data and energy integrated communication networks (DEIN) and intelligent reflecting surface (IRS).

Kun Yang (F'23) received his PhD from the Department of Electronic & Electrical Engineering of University College London (UCL), UK. He is currently a Chair Professor in the School of Computer Science & Electronic Engineering, University of Essex, UK, leading the Network Convergence Laboratory (NCL). He is also an affiliated professor of Nanjing University and UESTC, China. His main research interests include wireless networks and communications, future Internet and edge computing. In particular he is interested in energy aspects of future communication systems such as 6G and new AI (artificial intelligence) technique for wireless. He has managed research projects funded by UK EPSRC, EU FP7/H2020, and industries. He has published 400+ papers and filed 30 patents. He serves on the editorial boards of a number of IEEE journals (e.g., IEEE TNSE, TVT, WCL). He is a Deputy Editor-in-Chief of IET Smart Cities Journal. He has been a Judge of GSMA GLOMO Award at World Mobile Congress – Barcelona since 2019. He was a Distinguished Lecturer of IEEE ComSoc (2020-2021). He is a Member of Academia Europaea (MAE), a Fellow of IEEE, a Fellow of IET and a Distinguished Member of ACM.

Kezhi Wang received the Ph.D. degree from the University of Warwick, U.K. He is a Senior Lecturer with the Department of Computer Science, Brunel University London, U.K. His research interests include wireless communications, mobile edge computing, and machine learning. He is a co-recipient of IEEE ComSoc Leonard G. Abraham Prize (2022) and IEEE ComSoc Heinrich Hertz Award (2023).

Guopeng Zhang received the Ph.D. degree from the School of Communication Engineering, Xidian University, Xi'an, China, in 2009. He is currently a Professor with the School of Computer Science and Technology, China University of Mining and Technology, Xu'zhou, China. He has authored or co-authored more than 60 journal and conference papers. His main research interests include distributed machine learning, data mining, and mobile edge computing.